Journal of Medicinal Chemistry

Article

pubs.acs.org/jmc

Novel Tacrine−Benzofuran Hybrids as Potent Multitarget-Directed Ligands for the Treatment of Alzheimer's Disease: Design, Synthesis, Biological Evaluation, and X-ray Crystallography

Xiaoming Zha,[*,†,¶] Doriano Lamba,[‡,¶] Lili Zhang,[†,§] Yinghan Lou,[†,∥] Changxu Xu,[†,§] Di Kang,[†,∥] Li Chen,[§] Yungen Xu,[∥] Luyong Zhang,[†] Angela De Simone,[⊥] Sarah Samez,[‡,#] Alessandro Pesaresi,[‡] Jure Stojan,[▽] Manuela G. Lopez,[○] Javier Egea,[○] Vincenza Andrisano,[⊥] and Manuela Bartolini[*,◆]

[†]State Key Laboratory of Natural Medicines and Jiangsu Key Laboratory of Drug Screening, China Pharmaceutical University, 24 Tongjiaxiang, Nanjing 210009, P. R. China

[‡]Istituto di Cristallografia, Consiglio Nazionale delle Ricerche, Area Science Park - Basovizza, S.S. no. 14 Km 163.5, I-34149 Trieste, Italy

[§]Department of Natural Medicinal Chemistry, [∥]Department of Medicinal Chemistry, China Pharmaceutical University, 24 Tongjiaxiang, Nanjing 210009, P. R. China

[⊥]Department for Life Quality Studies, University of Bologna, Corso d'Augusto 237, I-47921 Rimini, Italy

[#]Dipartimento di Scienze Chimiche e Farmaceutiche, Università di Trieste, Via L. Giorgieri 1, I-34127 Trieste, Italy

[▽]Institute of Biochemistry, Medical Faculty, University of Ljubljana, Vrazov trg 2, SI-1000 Ljubljana, Slovenia

[○]Instituto Teófilo Hernando, Department of Pharmacology, Universidad Autónoma de Madrid, C/Arzobispo Morcillo 4, 28029 Madrid, Spain

[◆]Department of Pharmacy and Biotechnology, University of Bologna, Via Belmeloro 6, I-40126 Bologna, Italy

Supporting Information

ABSTRACT: Twenty-six new tacrine−benzofuran hybrids were designed, synthesized, and evaluated in vitro on key molecular targets for Alzheimer's disease. Most hybrids exhibited good inhibitory activities on cholinesterases and β-amyloid self-aggregation. Selected compounds displayed significant inhibition of human β-secretase-1 (*h*BACE-1). Among the 26 hybrids, **2e** showed the most interesting profile as a subnanomolar selective inhibitor of human acetylcholinesterase (*h*AChE) (IC_{50} = 0.86 nM) and a good inhibitor of both β-amyloid aggregation (*h*AChE- and self-induced, 61.3% and 58.4%, respectively) and *h*BACE-1 activity (IC_{50} = 1.35 μM). Kinetic studies showed that **2e** acted as a slow, tight-binding, mixed-type inhibitor, while X-ray crystallographic studies highlighted the ability of **2e** to induce large-scale structural changes in the active-site gorge of *Torpedo californica* AChE (*Tc*AChE), with significant implications for structure-based drug design. In vivo studies confirmed that **2e** significantly ameliorates performances of scopolamine-treated ICR mice. Finally, **2e** administration did not exhibit significant hepatotoxicity.

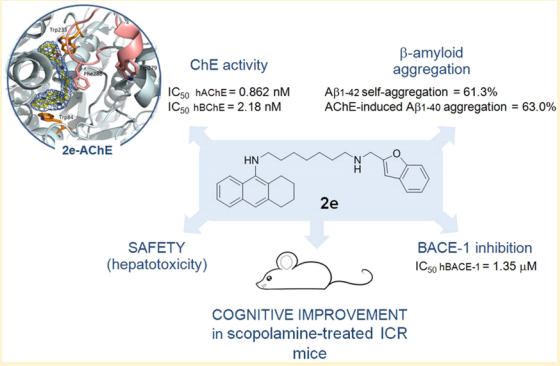

INTRODUCTION

Alzheimer's disease (AD) is an age-related neurodegenerative disorder with a known multifactorial etiopathology in which genetic, environmental, and endogenous factors, including protein misfolding and aggregation, oxidative stress, mitochondrial abnormalities, and neuroinflammation, all play a role. The impact of this pathology in developed countries with increasing aging population is tremendous.[1] According to the Alzheimer's Association, AD is the only one of the top 10 causes of death in the United States without a means to prevent, cure, or slow its progression. Notwithstanding the clear need for an effective therapeutic treatment, the drugs currently on the market merely stabilize some symptoms of early to-midstage forms of AD for a limited period of time. Although several research strategies have been envisaged in recent decades, increasing cholinergic neurotransmission by inhibiting the enzyme acetylcholinesterase (AChE) still represents one of the mainstream treatment options for AD. Cholinesterase inhibitors (ChEIs) temporally restore native levels of the neurotransmitter acetylcholine (ACh), which compensates for the cholinergic impairment caused by extensive degeneration of the cholinergic neurons

Received: July 16, 2015
Published: December 3, 2015

DOI: 10.1021/acs.jmedchem.5b01119
J. Med. Chem. 2016, 59, 114−131

and the loss of cholinergic transmission in brain areas. However, the cholinergic deficit is just one of the hallmarks of the AD pathology. The complex interconnection of the molecular events underpinning AD is thought to be one of the reasons that the single-target directed drugs that have reached clinical trials have failed. This complexity implies that the success of a therapeutic approach is likely to depend on the simultaneous modulation of more than one pathological target, which has led to a new paradigm in drug discovery for AD, namely the development of multifunctional molecules as multitarget direct ligands (MTDLs). MTDLs with two or more complementary biological activities have been shown to offer important advances toward effective treatment, and several research groups have contributed to their development.[2−5] MTDLs may be generated by combining fragments endowed with complementary properties, each fragment synergistically contributing to the overall activity profile of the resulting molecule.

One hallmark of AD is the presence in the hippocampus of senile plaques, which are primarily formed by the extracellular deposition of β-amyloid peptides (Aβ). Although there is still debate on the interconnection with other AD hallmarks, Aβ oligomerization and aggregation are thought to play a key role in AD pathogenesis and progression. Aβ is a 39−42 amino acid peptide, which is generated from the amyloid precursor protein (APP) via sequential cleavage by two enzymes, β-secretase (also called β-site APP cleaving enzyme, BACE-1) and γ-secretase. Thus, inhibiting Aβ generation by hindering BACE-1 activity and/or inhibiting Aβ oligomerization and aggregate accumulation have both been envisaged as suitable strategies for AD treatment.

To achieve a new family of MTDL hybrid molecules with anticholinesterase activity, the framework of the well-known cholinesterase inhibitor tacrine (1,2,3,4-tetrahydroacridine-9-amine) was selected. Until recently, AChE inhibition has been mainly associated with alleviation of AD symptoms, but AChE seems to also be implicated in AD pathogenesis by influencing Aβ deposition, as demonstrated both in vitro[6] and in vivo.[7] Furthermore, a relationship between AChE inhibitors (AChEIs) and the APP processing has been suggested, based on evidence that AChEIs possibly affect the expression and/or the metabolic processing of the APP and, consequently, may influence Aβ generation.[8,9] Finally, recent studies have shown that selective AChE/butyrylcholinesterase (BChE) inhibitors can reduce Aβ-induced inflammatory processes,[10] thus opening a new route for anticholinesterase inhibitors in AD treatment. On the basis of the recently discovered role played by AChE, developing MTDLs with AChE inhibitory activity is therefore still of interest. However, when designing hybrids containing a 1,2,3,4-tetrahydroacridine-9-amine unit, the issue of hepatotoxicity must be taken into consideration. Although hepatotoxicity associated with the administration of tacrine has limited its clinical use,[11] recent findings have shown that the safety can be improved by synthesizing tacrine derivatives and homo- and heterodimers.[12−20] Thus, provided that the lack of significant hepatotoxicity is proven, in our opinion, the tethahydroacridine scaffold still represents a powerful starting point to achieve multipotent derivatives.

Furthermore, a number of new lines of evidence have suggested that inhibitors of both cholinesterase enzymes may have beneficial functions in AD. Indeed, in a healthy human brain, BChE mainly plays a secondary role in the hydrolysis of ACh, while in an AD brain, its role becomes predominant with AD progression as AChE levels decline and BChE levels rise.[21] More importantly, in vivo experiments showed that brain-targeted BChE inhibitors not only improved the cognitive performance of aged rats without the classic adverse effects associated with AChE inhibition but they also lowered Aβ brain levels in transgenic mice overexpressing human mutant APP[22] and ameliorated the Aβ-induced cognitive dysfunction in mice.[23]

Thus, considering the widened biological profile toward amyloid aggregation, the benzofuran nucleus (and the modification thereof) was selected as the framework to build new MTDLs. Some benzofuran derivatives have previously been shown to act as an AChEI[24] or as an inhibitor of Aβ fibril formation in vitro[25,26] and to reduce aggregated Aβ in the brain.[27,28] Furthermore, some 2-arylbenzofuran derivatives[29] and benzofuran−chalcone hybrids[30] were recently characterized in vitro as MTDL agents. Finally, an aminostyrylbenzofuran derivative was shown to reduce amyloid oligomers and ameliorate the cognitive deficit in a transgenic mouse model for AD.[31]

On the basis of these promising new developments, herein we report on the design, synthesis, and biological evaluation of 26 new benzofuran hybrids (**1a−3h**). The rationale behind designing MTDLs is basically to achieve a balance among the different structural requirements for the optimal interaction with each selected target. Therefore, in an attempt to obtain a suitable activity profile against all the selected targets, i.e., BACE-1 as well as ChEs and Aβ aggregation, the influence of an amido vs amino linkage at the benzofuran unit was investigated [series **1** (**1a−1l**) and **2** (**2a−2f**), respectively]. The importance of a functional moiety able to hydrogen bond with the Asp dyad (Asp32/Asp228) of BACE-1 has been demonstrated.[32] According to recent work by Viayna et al.,[33] compounds bearing an aminoquinoline system may establish electrostatic interactions with the catalytic dyad that could stabilize the inhibitor−enzyme complex. Furthermore, while the presence of a properly spaced protonable amino group and aromatic residues should facilitate the interaction with the AChE's peripheral anionic site (PAS), the introduction of an amido group coupled with aromatic planar moieties may enhance the binding properties toward BACE-1.[34] Finally, thanks to the synthetic accessibility, series **3** (**3a−3h**), which includes hybrids bearing two benzofuran nuclei, was investigated. Indeed, the presence of larger substituent may improve the inhibitory activity against Aβ aggregation as well as against BACE-1. In fact, the relatively large β-secretase active site can accommodate bulky molecules and represents an additional challenge for designing potent nonpeptidic inhibitors.[34]

Characterizing the biological activity includes: (i) evaluating the in vitro inhibitory activity against human cholinesterase enzymes, (ii) investigating the mechanism of action on AChE via in-solution kinetic studies, (iii) assessing the binding mode of the most active derivative by elucidating the crystal structure of the inhibitor−AChE complex via X-ray diffraction (XRD), (iv) assessing the in vivo activity of the most promising derivative in scopolamine-treated ICR mice, and (v) evaluating the in vitro ability to interfere with Aβ production and aggregation by studying the effects on BACE-1 activity (via a FRET-based assay) and both $A\beta_{1-42}$ self-aggregation and AChE-induced $A\beta_{1-40}$ aggregation (via fluorescence assays). Finally, to address the critical hepatotoxicity issue related to the presence of the tacrine unit, the hepatotoxicity of the most

DOI: 10.1021/acs.jmedchem.5b01119
J. Med. Chem. 2016, 59, 114−131

Scheme 1. Synthesis of Compounds 1a−1l, 2a−2f, and 3a−3h[a]

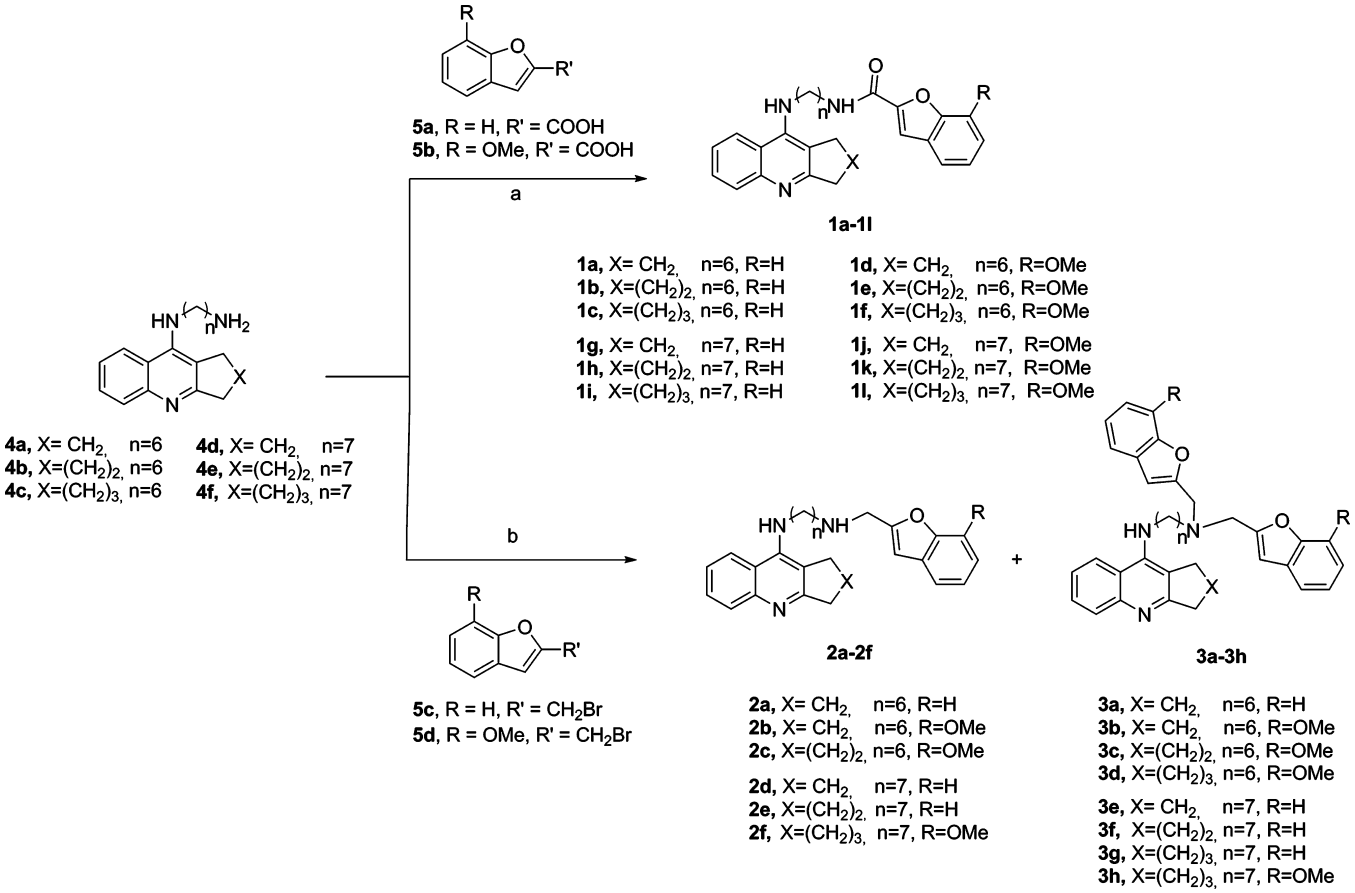

[a]Reagents and conditions: (a) *N,N′*-carbonyl diimidazole, THF, rt, 4 h; (b) K_2CO_3, KI, CH_2Cl_2, rt.

Scheme 2. Synthesis of Intermediate 4f[a]

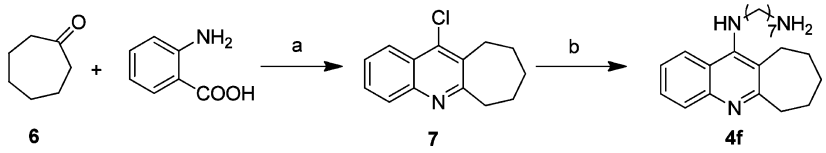

[a]Reagents and conditions: (a) $POCl_3$, reflux, 3 h; (b) pentanol, $NH_2(CH_2)_7NH_2$, reflux, 18 h.

interesting derivative was evaluated by monitoring the plasma levels of two serum biomarkers for acute liver injury.

RESULTS AND DISCUSSION

Chemistry. The synthesis of the hybrids **1a−3h** is depicted in Scheme 1. The amines **4a−4e**[18,35−37] and **4f** were treated with the acids **5a** and **5b**[38,39] and *N,N′*-carbonyl diimidazole in dry THF at rt to yield series **1** (**1a−1l**). Derivatives **4a−4f** were reacted with the bromides **5c** and **5d**[40] using KI and K_2CO_3 in dry CH_2Cl_2 to yield series **2** (**2a−2f**) and **3** (**3a−3h**).

The compound **4f** was obtained from anthranilic acid and cycloheptanone (**6**). The product 11-chloro-7,8,9,10-tetrahydro-6*H*-cyclohepta[*b*]quinoline (**7**) was treated with 1,7-diaminoheptane. The procedure is reported in Scheme 2.

Biological Evaluation. *AChE and BChE Inhibition.* The inhibitory potency of compounds **1a−1l**, **2a−2f**, and **3a−3h** was assessed by Ellman's assay on recombinant human AChE (*h*AChE) and BChE from human serum (*h*BChE).[41] The IC_{50} values were compared with those obtained for the reference compounds tacrine and bis(7)-tacrine, a tacrine dimer with multiple neuroprotective activities, including concurrent inhibition of cholinesterase enzymes, Aβ cascade, and related toxicity and the reduction of hydrogen peroxide-induced cell injury.[42−46] The IC_{50} values of all the compounds tested against *h*AChE and *h*BChE are summarized in Table 1.

The inhibitory activities of the 26 hybrids ranged from good to very potent against both cholinesterases. The IC_{50} values for *h*AChE inhibition ranged from micromolar to subnanomolar, from 7.49 μM to 0.86 nM. Specifically, hybrids with the general structure **1** had inhibitory activities from 24.4 nM to 1.685 μM. The presence of either a cyclopentane (**1a**) or cycloheptane (**1c**) ring in place of a cyclohexane ring (**1b**) only slightly affected the anti-*h*AChE activity of the hybrids bearing a six-carbon tether chain. However, the concomitant introduction of a methoxy substituent on the benzofuran moiety increased the inhibitory potency by an order of magnitude for hybrids with either a cycloheptane [X = $(CH_2)_3$] or a cyclohexane [X = $(CH_2)_2$] ring (**1b** vs **1e** and **1c** vs **1f**). This effect was less

DOI: 10.1021/acs.jmedchem.5b01119
J. Med. Chem. 2016, 59, 114−131

Table 1. Inhibition of *h*AChE and *h*BChE, Selectivity Ratio, and Inhibition of A$\beta_{1\text{-}42}$ Self-Aggregation

compd	X	R	n	*h*AChE IC_{50} (nM) ± SEM[a]	*h*BChE IC_{50} (nM) ± SEM[a]	selectivity ratio[b]	inhibition of Aβ_{1-42} self-aggregation (% ± SEM)[c]
1a	CH_2	H	6	545 ± 35	15.7 ± 1.4	0.029	18.7 ± 4.3
1b	$(CH_2)_2$	H	6	424 ± 21	4.68 ± 0.19	0.011	13.7 ± 0.2
1c	$(CH_2)_3$	H	6	308 ± 34	10.8 ± 0.6	0.035	24.2 ± 0.8
1d	CH_2	OCH_3	6	1,685 ± 33	80.6 ± 5.4	0.048	32.6 ± 9.8
1e	$(CH_2)_2$	OCH_3	6	24.4 ± 0.4	10.2 ± 1.0	0.418	40.2 ± 5.6
1f	$(CH_2)_3$	OCH_3	6	32.3 ± 0.9	30.0 ± 1.9	0.929	18.7 ± 5.4
1g	CH_2	H	7	48.6 ± 2.7	30.9 ± 2.3	0.636	10.2 ± 4.3
1h	$(CH_2)_2$	H	7	76.9 ± 6.3	6.90 ± 0.25	0.090	26.2 ± 0.5
1i	$(CH_2)_3$	H	7	323 ± 25	11.6 ± 0.7	0.036	17.3 ± 1.7
1j	CH_2	OCH_3	7	993 ± 72	26.1 ± 1.0	0.026	19.6 ± 1.1
1k	$(CH_2)_2$	OCH_3	7	44.2 ± 3.3	7.35 ± 0.40	0.166	42.5 ± 2.5
1l	$(CH_2)_3$	OCH_3	7	416 ± 5	31.9 ± 1.4	0.077	17.7 ± 2.5
2a	CH_2	H	6	47.0 ± 5.5	2.48 ± 0.24	0.053	9.3 ± 1.8
2b	CH_2	OCH_3	6	63.1 ± 5.6	1.30 ± 0.14	0.021	64.1 ± 6.5
2c	$(CH_2)_2$	OCH_3	6	15.3 ± 1.1	0.49 ± 0.03	0.032	52.0 ± 4.5
2d	CH_2	H	7	10.8 ± 0.8	2.54 ± 0.25	0.235	76.2 ± 5.1
2e	$(CH_2)_2$	H	7	0.86 ± 0.05	2.18 ± 0.25	2.535	61.3 ± 4.5
2f	$(CH_2)_3$	OCH_3	7	2.56 ± 0.16	1.23 ± 0.07	0.481	31.9 ± 11.3
3a	CH_2	H	6	2,070 ± 225	8.89 ± 0.53	0.004	62.2 ± 3.2
3b	CH_2	OCH_3	6	7,495 ± 345	2.30 ± 0.14	0.0003	38.5 ± 1.3
3c	$(CH_2)_2$	OCH_3	6	260 ± 65	0.48 ± 0.06	0.002	44.6 ± 2.1
3d	$(CH_2)_3$	OCH_3	6	1,036 ± 115	2.35 ± 0.15	0.002	25.0 ± 2.6
3e	CH_2	H	7	222 ± 23	12.8 ± 1.5	0.058	30.7 ± 2.4
3f	$(CH_2)_2$	H	7	117 ± 8	6.86 ± 0.56	0.059	44.5 ± 3.5
3g	$(CH_2)_3$	H	7	200 ± 8	17.9 ± 2.3	0.090	39.8 ± 9.1
3h	$(CH_2)_3$	OCH_3	7	199 ± 13	4.87 ± 0.20	0.025	37.3 ± 5.8
tacrine				424 ± 21	45.8 ± 3.0	0.108	<5
bis(7)-tacrine				0.81 ± 0.09	5.66 ± 0.15	6.988	50.1 ± 2.3

[a]Recombinant human AChE and BChE from human serum were used. Data are the mean of at least three independent determinations. [b]Selectivity ratio = IC_{50} *h*BChE/IC_{50} *h*AChE. [c]Inhibition of A$\beta_{1\text{-}42}$ self-aggregation investigated by the thioflavin-T fluorescence assay. Assays were carried out in the presence of 10 μM inhibitor and 50 μM A$\beta_{1\text{-}42}$.

pronounced for hybrids bearing a seven-carbon tether chain. Conversely, for the cyclopentane analogues [X = CH_2], the introduction of the methoxy group decreased the inhibitory activity (**1a** vs **1d** and **1g** vs **1j**). The varying results can possibly be ascribed to the various positions of the benzofuran unit at the entrance to the AChE gorge depending on the structure of the quinoline fragment (see the X-ray crystallography section for the binding mode).

Concerning the effect of the spacer chain length on the anti-AChE activity, the optimal tether was a seven-carbon chain for the benzofuran hybrids bearing a tacrine unit or a 2,3-dihydro-1*H*-cyclopenta[*b*]quinoline unit. Indeed, by lengthening the tether chain from six to seven carbon units, the inhibitory activity against *h*AChE increased from 5.5- to 11-fold. However, for the cycloheptane analogues, the length of the tether chain did not strongly affect the anti-AChE activity (**1c** vs **1i**). Concerning the methoxybenzofuran hybrids, a slightly different trend was observed. Indeed, lengthening the tether chain to seven carbon units was beneficial for hybrids with the 2,3-dihydro-1*H*-cyclopenta[*b*]quinoline unit (the potency increased by a factor of 1.7, **1d** vs **1j**) but was detrimental for hybrids bearing a tacrine unit or a 7,8,9,10-tetrahydro-6*H*-cyclohepta[*b*]quinoline unit (the potency decreased by a factor of 1.8 and 12.9, respectively).

The introduction of an amino group in the spacer chain in series **2** lead to some of the most potent *h*AChE inhibitors synthesized in this work, with IC_{50} values in the low nanomolar−subnanomolar range. Indeed, the presence of an amino group in the spacer chain may have enabled π−cation interaction with the PAS, greatly enhancing the anti-AChE activity (e.g., **2e** is 89 times more potent than its amido analogue **1h**). The optimal linker for anti-AChE activity was a seven-carbon chain. The most potent hybrid (**2e**) showed a subnanomolar inhibitory potency and was approximately 493 times more potent than tacrine and equipotent to the reference compound bis(7)-tacrine. **2e** was also the only derivative slightly selective for *h*AChE (2.5-fold).

Finally, in series **3**, the introduction of the second benzofuran unit in hybrids **3a**−**3h** decreased the anti-AChE activity by 1−2 orders of magnitude (e.g., **2a** vs **3a** or **2d** vs **3e**). Because AChE would poorly accommodate bulky inhibitors, this detrimental effect was more evident for *h*AChE than for *h*BChE. Indeed, the volumes of the upper portions of the *Torpedo californica* AChE (*Tc*AChE) and *h*AChE catalytic gorges are 812 and 790 Å^3, respectively, while that of *h*BChE is as high as 1133 Å^3. The unfavorable effect of the bulkier fragment was worse for hybrids with a six-carbon tether than for hybrids with a seven-carbon chain (**3a** vs **3e** or **3d** vs **3h**). Lengthening the tether chain by one carbon unit reduced the unfavorable effect of the second benzofuran unit by almost 1 order of magnitude. For hybrids within series **3**, the presence or absence of a methoxy residue on the benzofuran moiety had only a weak influence on the inhibitory activity (**3a** vs **3b**, **3g** vs **3h**).

DOI: 10.1021/acs.jmedchem.5b01119
J. Med. Chem. 2016, 59, 114−131

To properly rank the anticholinesterase activity of these new hybrids in the scenario of tacrine-based MTDLs, a comparison can be made with tacrine heterodimers published within the last two years. Compared with the recently published tacrine hybrids, **2e** is 17.9 times more potent than the best coumarin−tacrine derivative reported by Hamulakova S. et al. (15.4 nM),[47] 25.6 times more potent than the rhein−tacrine hybrid developed by Li et al. (22.0 nM, on AChE from electric eel),[35] slightly more potent than rhein−huprine derivatives reported by Viayna et al. (2.39 nM),[33] 103 times more potent than the best phenothiazine−tacrine hybrid (89 nM),[48] and similar in potency to a recently published quinone−tacrine hybrid (0.72 nM).[17]

However, it is worth mentioning that, in an MTDL framework, a strong AChE inhibitory activity is only part of the rationale behind the development of such molecules.

Because of its role in the AD brain, the inhibitory potency against *h*BChE was also evaluated and reported in Table 1. Within the brain, BChE is primarily expressed and secreted by glial cells[49] and it is thought to play a compensatory role in response to the decrease of AChE activity in the brain as AD progresses.[50] Indeed, inhibition of central BChE activity has also been investigated as a potential therapeutic approach to ameliorate the cholinergic deficit in moderate forms of AD.[51]

All benzofuran hybrids proved to be potent and selective *h*BChE inhibitors (except for **2e**). The IC_{50} values against *h*BChE ranged from 0.478 to 80.6 nM. The most selective *h*BChE inhibitors belonged to series **3** (**3a**−**3d**, with selectivity ratios from 2 to 3 orders of magnitude) and were characterized by a hexamethylene chain. Removing one of the 7-methoxybenzofuran fragments reduced the selectivity for *h*BChE by 67-fold (**2b** vs **3b**). However, the lower selectivity of **2b**, which lacks the second benzofuran unit, is a consequence of a higher inhibitory potency against *h*AChE rather than a higher anti-*h*BChE activity, which can be ascribed to lower steric hindrance. Indeed, because the volume of the upper portion of the *h*BChE catalytic gorge is approximately 340 $Å^3$ larger than the corresponding portion of the *h*AChE gorge, *h*BChE should better accommodate the two benzofuran fragments. Consequently, the introduction of the second methoxybenzofuran unit either did not affect (e.g., **2c** vs **3c**) or only slightly decreased (e.g., **2a** vs **3a**, **2b** vs **3b**) the inhibitory potency against *h*BChE. As opposed to what was observed for the inhibition of *h*AChE, one of the most potent *h*BChE inhibitor of series **3** (hybrid **3c**) bore a hexamethylene chain.

Among the hybrids belonging to series **3** and **2**, higher *h*BChE inhibitory activity was associated with the presence of a 7-methoxy substituent on the benzofuran nucleus (**3a** vs **3b**, **3g** vs **3h** and **2a** vs **2b**). For compounds within series **1** that carried an amido group at the interconnection between the spacer chain and the benzofuran fragment, this relationship was lost. The results also confirmed that both downsizing and enlarging the cyclohexane nucleus of the tacrine unit negatively affected the inhibitory potency against *h*BChE.

The highest *h*BChE inhibition was achieved with compounds **2c** and **3c**, whose IC_{50} values fall in the subnanomolar range (0.49 and 0.48 nM, respectively). Both compounds were characterized by the presence of a tacrine unit, a hexamethylene chain, and two 7-methoxy-benzofuran units, which were therefore key structural features for optimal *h*BChE inhibition.

The importance of the selectivity for one of the two cholinesterase enzymes by the tacrine−benzofuran hybrids deserves a final comment. Considering that the roles played by AChE and BChE in the modulation of the central cholinergic tone vary with the progression of the disease, where the role of BChE progressively increases as AChE levels decrease, it is conceivable that selective AChEIs are more effective in the early stages of AD, when AChE still plays a major role. Conversely, nonselective and BChE-selective inhibitors may be more effective in moderate to severe forms of AD. Thus, the complex scenario of this pathology, together with an incomplete understanding of the "nonclassical" roles played by each of these two enzymes, makes the development of centrally active cholinesterase inhibitors selective for either AChE or BChE a worthy avenue to investigate.

Kinetic Study of Human AChE Inhibition. In the last two decades, the ability of cholinesterase inhibitors to interact with the PAS of AChE has attracted attention for the development of a new disease-modifying drug able to interfere with the pro-aggregating action of AChE on β-amyloid peptides, possibly exerted through the interaction of Aβ with PAS.[52] Thus, the ability of this series of hybrids to act as dual binding site AChE inhibitors was investigated.

In vitro studies on the isolated enzyme were carried out using recombinant *h*AChE and **2e**. The mechanism of action was evaluated by building a Lineweaver−Burk double reciprocal plot at increasing inhibitor and substrate concentrations. Overlaid reciprocal Lineweaver−Burk plots showed both higher slopes (decreased V_{max}) and intercepts (higher K_m) at increasing inhibitor concentrations (Figure 1), a trend that is

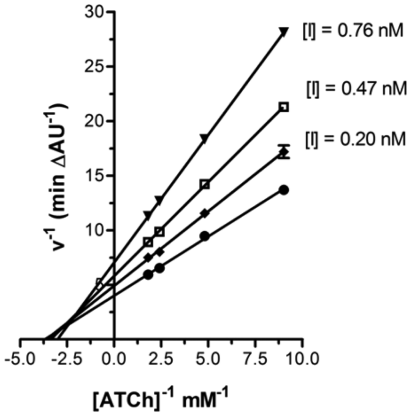

Figure 1. Kinetic study on the mechanism of *h*AChE inhibition by **2e**. Overlaid Lineweaver−Burk reciprocal plots of the AChE initial velocity at increasing substrate (acetylthiocholine, ATCh) concentrations (ATCh < 0.56 mM) in the absence and in the presence of **2e** (0−0.76 nM) are shown. Lines were derived from a weighted least-squares analysis of the data points.

generally ascribed to a mixed-type inhibition. The mixed-type mechanism of action was also confirmed by a Cornish−Bowden plot (data not shown). The inhibitor dissociation constants K_i and the dissociation constant for the enzyme−substrate−inhibitor complex K'_i were estimated to be 0.72 and 1.04 nM, respectively.

X-ray Crystallography of *Tc*AChE−2e Complex. To gain insights into the molecular determinants responsible for the high activity of **2e** (Figure 2A), the crystal structure of the inhibitor-bound *Tc*AChE (Figure 2B) was determined by X-ray crystallography at 2.8 Å resolution (summary of Crystallo-

DOI: 10.1021/acs.jmedchem.5b01119
J. Med. Chem. 2016, 59, 114−131

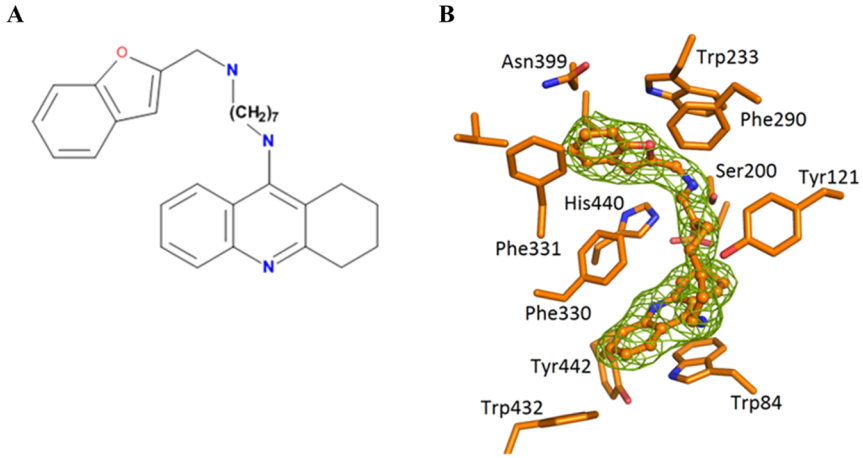

Figure 2. (A) Molecular structure of compound **2e**. (B) Close-up view of the active site of *Tc*AChE complexed with **2e**. The final $2F_o - F_c$ σA-weighted electron density map is contoured at 1.0σ. **2e** is rendered as a ball and stick model with carbon, oxygen, and nitrogen atoms colored orange, red, and blue, respectively. Selected key protein residues (C_α atoms and side chains) in the vicinity of **2e** are rendered in stick format and labeled appropriately. Hydrogen bonding interactions have been omitted for clarity. Part B was created using PyMOL (http://www.pymol.org).

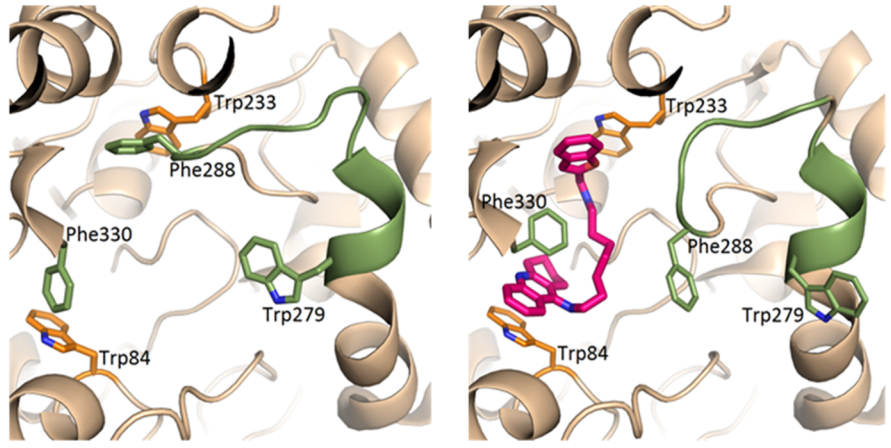

Figure 3. Conformational plasticity of the Trp279–Phe290 loop. (A) Conformation of the Trp279–Phe290 loop and orientation of the Phe330 side chain in the *Tc*AChE apo structure (PDB ID 1EA5). (B) Conformational adaptation of the Trp279–Phe290 loop and orientation of the Phe330 side chain upon binding of **2e** to *Tc*AChE. Selected key protein residues (C_α atoms and side chains) are rendered in stick format and labeled appropriately. Created using PyMOL (http://www.pymol.org).

graphic Data of the *Tc*AChE–**2e** complex in Supporting Information, Table S1).

Crystallographic studies of AChE have been carried out on *Torpedo californica*, mouse, or human homologues. Of the 165 AChE structures deposited in the Protein Data Bank, there are 82 *Torpedo californica*, 70 mouse, and 13 human AChE structures. A comparative amino acid sequence analysis indicates an overall 57% identity and 75% similarity between *Tc*AChE and *h*AChE. The 44 residues of the catalytic gorge share an even higher sequence identity and a similarity of 77% and 91%, respectively, which validates *Tc*AChE as an accurate alternative to *h*AChE for the present structural study of drug binding.

The position and orientation of **2e** with respect to the key residues in the *Tc*AChE active-site gorge confirmed the critical role of the tacrine fragment, which binds at the anionic site by stacking against the aromatic rings of Trp84 and Phe330. The conformation of Phe330 in the *Tc*AChE–**2e** complex (χ_1 = 92.6°, χ_2 = −68.6°) was found to be significantly different than those observed in the apo *Tc*AChE[53] (PDB ID 1EA5) and in the aged phosphonylated *Tc*AChE (PDB ID 2DFP)[54] as well as in the *Tc*AChE–tacrine[55] (PDB ID 1ACJ), *Tc*AChE–bis(5)-tacrine[56] (PDB ID 2CMF) and *Tc*AChE–bis(7)-tacrine[56] (PDB ID 2CKM) complexes. In the *Tc*AChE–**2e** complex, the swinging gate residue Phe330 closely matches one of the two alternative conformations observed in the *Tc*AChE–NF595 [(*N*-(1,2,3,4-tetrahydroacridin-9-yl)-8-[(1,2,3,4-tetrahydroacridin-9-yl)thio]octan-1-amine)] (PDB ID 2CEK) complex (χ_1 = 76.1°, χ_2 = −72.6°).[57]

The endocyclic nitrogen of **2e** is hydrogen bonded to the main-chain carbonyl oxygen (2.76 Å) of the catalytic residue His440 (Figure 2B). It can be inferred from this distance and the pK_a of tacrine (9.8)[58] that the tacrine moiety of **2e** is protonated. The distance between Ser200-O_γ and His440-$N_{\varepsilon 2}$ of 3.4 Å indicates that the catalytic triad is disrupted. Indeed, Ser200-O_γ is shifted toward the oxyanion hole and interacts with the main chain nitrogen atoms of the Ala201 (2.8 Å), Gly118 (3.4 Å), and Gly119 (3.7 Å) residues, which in turn do not significantly shift from their position in the apo structure.[53] A protonated *N*-alkyl tacrine would be expected to have

DOI: 10.1021/acs.jmedchem.5b01119
J. Med. Chem. 2016, 59, 114–131

maximal resonance stabilization if the *N*-alkyl substituent were roughly coplanar with the ring system. In the *Tc*AChE−**2e** complex, an intermediate dihedral angle of 133.7° is observed for the tacrine fragment, i.e., 56.3° out of coplanarity. This value is consistent with those observed in the crystal structures of complexes with *Tc*AChE.[33] Interestingly, in the *Tc*AChE−**2e** complex, the exocyclic NH_2 group of **2e** is not involved in hydrogen bonding, with the otherwise structurally conserved water molecules belonging to the active site water network.

The alkyldiamine linker [$C_{quinolinium}$-NH-$(CH_2)_7$-NH-$CH_{2benzofuran}$] between the quinolinium and the methylbenzofuran substructures adopts a conformation not previously reported, namely a (−)anticlinal (−111.7°), (+)synclinal (39.5°), (+)anticlinal (137.1°), (+)anticlinal (140.9°), (+)-synclinal (80.7°), (+)anticlinal (111.1°), (+)anticlinal (127.9°), antiperiplanar (155.2°), and synperiplanar (8.1°) conformation. Strikingly, this allows a close interaction (2.39 Å) between the Ser200-O_γ and the distal nitrogen (NWA) of the alkyldiamine linker (Supporting Information, Figure S1).

In the *Tc*AChE−**2e** complex, the displacement of the main-chain atoms of Phe331 (0.4 Å) toward the opening of the gorge is not significant compared with that observed in the structure of the apo *Tc*AChE[53] and the above-mentioned complexes,[54−57] except for the *Tc*AChE−bis(5)-tacrine complex[56] (1.0 Å). On the other hand, the position/orientation of the Phe331 phenyl ring is significantly different from those observed in the above-mentioned structures.[53−57] This has dramatic consequences on the position/orientation and the overall conformation of the loop encompassing the residues from Trp279 to Phe290, which bears residues of both the PAS and the acyl pocket (Supporting Information, Figures S2A and S2B).

The reorientation of the Phe331 side chain (χ_1 = 168.0°, χ_2 = −85.6°) compared with those observed in the apo *Tc*AChE,[53] *Tc*AChE−tacrine,[55] *Tc*AChE−bis(7)-tacrine[56] and, to some extent, in the *Tc*AChE−NF595[57] complex, disrupts its stacking interaction with Phe288, as previously reported for *Tc*AChE−bis(5)-tacrine[56] and for aged phosphonylated *Tc*AChE.[54]

The largest structural alterations upon the binding of **2e** to *Tc*AChE are observed in the Trp279−Phe290 loop (Figure 3).

The backbone atoms in this region are displaced as much as 6.0 Å (C_α-Phe288) from their native positions,[53] with the side chains dramatically reoriented, while in the *Tc*AChE−bis(5)-tacrine[56] and in the aged phosphonylated *Tc*AChE[54] structures the observed displacements are as high as 4.8 Å (C_α-Asp285) and 4.6 Å (C_α-Arg289), respectively (Supporting Information, Figure S2B).

An alternative conformation of the Trp279−Phe290 loop with respect to that of the apo structure (Figure 3A) was already observed in *Tc*AChE complexed with a bifunctional derivative of the alkaloid galanthamine (PDB ID 1W76).[59] The inherent flexibility of this loop has also been demonstrated in site-directed mutagenesis studies. Indeed, the mutation of the *Tc*AChE Leu282 to either Ser or Ala disrupted cross-gorge interactions, which resulted in a substantial decrease in the enzyme's stability and, ultimately, the entire structure.[60] This rearrangement may explain the residual activity of the fasciculin/*Tc*AChE complex,[61] although molecular dynamics simulations have suggested that the occurrence of transient motions that would open or close alternative routes for the substrate access to the enzyme's active site would also maximize the inhibition of the enzyme.[62,63]

In the *Tc*AChE−**2e** complex, the 2-methylbenzofuran fragment displaces Phe288 outward from its position in the apo *Tc*AChE structure (Figure 3).[53] This shift largely occludes the entrance to the active-site gorge and accompanies a significant change in the main-chain conformation of the whole loop without disrupting the crystal packing. The 2-methyl-benzofuran fragment is nicely accommodated by a hydrophobic pocket formed by Trp233, Phe290, Phe330, Phe331, Val395, Asn399, and Val400. The orientation of the benzofuran ring is stabilized by a short nonbonded contact (3.3 Å) between the heterocyclic oxygen (OAY) and the $N_{\varepsilon 1}$ of the indole ring of Trp233.

Interestingly, in the structure of the *Tc*AChE−bis(5)-tacrine,[56] the rearrangement of the Trp279−Phe290 loop shifts the Phe331 toward the position occupied by Phe288 in the apo *Tc*AChE structure,[53] whereas in the conjugate of *Tc*AChE with the nerve agent, diisopropyl phosphofluoridate,[54] the isopropyl moiety of the organophosphoryl group, which is covalently bound to Ser200, displaces both Phe288 and Phe290 from their positions in the apo structure.[53]

The backbone atoms of Trp279 do not significantly differ from their native positions,[53] i.e., they differ by 0.4, 0.6, 0.2, and 0.7 Å in the *Tc*AChE−bis(5)-tacrine,[56] the aged phosphonylated *Tc*AChE,[54] the *Tc*AChE-NF595,[57] and *Tc*AChE−**2e** structures, respectively. On the other hand, the side chain of Trp279 is dramatically reoriented in the *Tc*AChE−**2e** complex (Figure 3B) with dihedral angles of χ_1 = 51.3° and χ_2 = −82.0° compared with those in the apo *Tc*AChE[53] (−62.3°, 96.7°), *Tc*AChE−bis(5)-tacrine[56] (−76.3°, 95.2°), the aged phosphonylated *Tc*AChE[54] (−56.2°, 99.4°), and the *Tc*AChE−NF595[57] (−118.2°, −131.9°) structures, respectively.

Kinetic Evaluation of Compound 2e on *Tc*AChE. To confirm the high inhibitory activity and gain further information about the mechanism of *Tc*AChE inhibition by **2e**, kinetic experiments were performed using a stopped-flow apparatus. The shape of the progress curves (Supporting Information, Figure S3) and the concentrations of the tested compound (1−10 nM) and *Tc*AChE (3.4 nM) used in the assay are typical for slow, tight-binding inhibition. This type of inhibition was further confirmed by potentiometric titration of **2e** (0.3 nM) with increasing enzyme concentrations (Supporting Information, Figure S4). The concave-upward shape of the residual activity plot obtained after 90 min of preincubation indicates tight-binding inhibition, with the linear portion of the plot extrapolating exactly to the added **2e** concentration of 0.3 nM.

The atypical shape of the progress curves, with the kink appearing earlier as the inhibitor concentration increases, was thoroughly tested by several kinetic models. To simplify the progress curve analysis, an ATCh concentration of 80 μM was used, at which the *Tc*AChE obeys the Michaelis−Menten relationship. Among the mechanisms tested, the best fitting was obtained with a model in which the inhibitor binds to both free and acetylated *Tc*AChE, confirming a mixed-type inhibition.

It has also been assumed that the observed slow inhibition is the effect of the slow binding of the inhibitor **2e** to the enzyme active site (k_{on} *competitive* 1.45 ± 0.70 × 10^7 M^{-1} s^{-1}; k_{off} *competitive* 0.0320 ± 0.0002 s^{-1}; k_{on} *non-competitive* 1.45 × 10^7 M^{-1} s^{-1}; k_{off} *noncompetitive* 0.0310 ± 0.0004 s^{-1}). This is the result of the low concentrations of the enzyme and inhibitor in a close stoichiometric ratio. Consequently, an instantaneous *Tc*AChE inhibition was not detected, and the kinetic analysis required a nonequilibrium treatment. The K_i values calculated

DOI: 10.1021/acs.jmedchem.5b01119
J. Med. Chem. 2016, 59, 114−131

for AChE inhibition by **2e** (K_i *competitive* = 2.2 nM; K_i *noncompetitive* = 2.1 nM) confirmed a nanomolar inhibitory potency. Similarly, compounds **1e**, **1f**, **1h**, and **3c** were assayed (results in SI, Table S2).

The reported *Tc*AChE−**2e** crystal structure reveals the structural basis for the high anti-AChE activity. Indeed, **2e** forms a favorable $\pi-\pi$ interaction with Trp84 via the tacrine fragment and disrupts the catalytic triad as a result of Ser200-O_γ hydrogen bonding with the distal nitrogen of the alkyldiamine linker.

Inhibition of AChE-Induced Aβ_{1-40} Aggregation. Growing experimental evidence has shown that PAS binders can inhibit some noncholinergic functions of AChE, including the AChE-induced Aβ oligomerization and fibrillization.[6,64] Given the ability of **2e** to contact PAS, its ability to inhibit AChE-induced Aβ_{1-40} aggregation was investigated by a thioflavin T-based fluorometric assay[6] and compared with that of bis(7)-tacrine. The results demonstrated that **2e** was able to reduce *h*AChE-induced amyloid fibrillization by 58.4% at 100 μM, similarly to bis(7)-tacrine (68.0%) and to a recently developed tacrine-6-ferulic acid (50.27%).[65] In the same experimental conditions, the drug tacrine was not able to inhibit AChE-induced Aβ_{1-40} aggregation to a significant extent.

On the basis of the binding mode of **2e** to AChE highlighted by X-ray crystallography, the inhibitory activity against AChE-induced Aβ_{1-40} aggregation is likely the result of the dramatic rearrangement of the Trp279−Phe290 loop encompassing the overall position and main-chain/side-chain conformations/orientations that occurs to accommodate the benzofuran moiety. This has dramatic consequences on the physicochemical properties of the affected molecular surface region so that the aggregation and deposition of the Aβ peptide is expected to be hampered.

Inhibition of Aβ Production and Self-Aggregation. The production and accumulation of oligomeric aggregates of Aβ are considered to play an important role in the pathogenesis of AD. Thus, the inhibition of Aβ production and oligomerization have been investigated as attractive therapeutic strategies to more efficiently combat AD. Two key targets have been considered: (i) BACE-1 activity and (ii) Aβ_{1-42} self-aggregation.

BACE-1 is involved in the rate-limiting step in the proteolytic cleavage of APP to generate Aβ, and it is considered a key target to lower cerebral Aβ levels and limit Aβ-associated neurotoxicity.[66] The long-term administration of a BACE-1 inhibitor to transgenic mice significantly suppressed Aβ levels and halted the age-related cognitive decline.[34] Both preclinical and early phase clinical studies have validated BACE-1 as a therapeutic target.[67] Because of the high cost of substrates and recombinant enzymes, the inhibitory activity of a small selection of the hybrids was investigated in vitro using a fluorometric assay.[68] The selection included the most potent hybrid against *h*AChE, namely **2e**, its analogue **3f** with two benzofuran moieties to investigate the importance of this additional fragment on the interaction with the enzyme active site, and its amido analogue **1k**. Finally, because of the interesting inhibitory activity of **3f** against BACE-1, the analogue **3c** was also assayed.

Remarkably, all the selected hybrids were good BACE-1 inhibitors with submicromolar IC_{50} values (Table 2). They all clearly showed a much higher inhibitory potency than the reference compound bis(7)-tacrine, with **3c** being 40 times more potent than bis(7)-tacrine. Note that the drug tacrine was previously shown to be inactive as a BACE-1 inhibitor.[69] Moreover, a mild inhibition of BACE-1 may limit toxic effects associated with the complete suppression of BACE-1 activity in vivo.[70,71] As a final remark, the performance of these hybrids parallels the known nonpeptidic BACE-1 inhibitors. Indeed, the most potent BACE-1 inhibitors, including those that have entered clinical trials,[72] are characterized by one- to two-digit nanomolar potencies.[73] Examples of MTDLs with good BACE-1 inhibitory activity are the quinone-bearing polyamine memoquin (IC_{50} = 0.108 μM),[74] a rhein−huprine hybrid (IC_{50} = 0.08 μM),[33] and a recently published dual BACE-1/GSK-3β inhibitor (18.03 μM).[75]

Table 2. Inhibition of *h*BACE-1 Activity by 1k, 2e, 3c, and 3f[a]

compd	*h*BACE-1 (IC_{50}, μM)
1k	0.43 ± 0.22
2e	1.35 ± 0.13
3c	0.19 ± 0.03
3f	0.62 ± 0.18
bis(7)-tacrine	7.50 ± 0.40[b]

[a]Recombinant *h*BACE-1 was used; the results are the mean of two independent experiments ± SEM. [b]From ref 77.

Molecular dynamic simulations of the rhein−huprine hybrids[33] suggest that, like the huprine Y moiety, the tacrine fragment can be accommodated in the binding site encompassing the BACE-1 catalytic pocket (sheltered by the highly flexible β-hairpin loop between Val67 and Glu77 commonly known as the "flap")[32] as a consequence of the likely electrostatic stabilization between the protonated aminoquinoline system of the hybrids **1k**, **2e**, **3c**, and **3f** and the catalytic dyad Asp32−Asp228. On the other hand, the benzofuran moiety (similarly to the hydroxyanthraquinone moiety) may fill the BACE-1 subsites S5−S7, which exhibit a remarkable preference for Trp and the hydrophobic residues in the P5−P7 positions of substrates/inhibitors.[76]

Indeed, the distance between the centroids of these binding sites is ca. 12 Å, a value that satisfies the geometrical criteria required for the tether of hybrids **1k**, **2e**, **3c**, and **3f**. The presence of the amido moiety in **1k** may account for the slightly higher inhibitory activity (compared with **2e**), which is likely to be capable to be engaged in an extra hydrogen bond (with the carbonyl acting as the acceptor).

The good *h*BACE-1 inhibitory activity of hybrids **3c** and **3f**, which both lack the extra hydrogen bonding capability, can be ascribed to the presence of an extra benzofuran moiety able to better fill the active site cleft between the N-terminal and C-terminal lobes of *h*BACE-1. The presence in **3c** of a more hydrophobic substituent on the benzofuran moiety (i.e., R = OMe, instead of H) may explain its slightly higher inhibitory activity against *h*BACE-1 than that exerted by **3f**.

Aβ_{1-42} is the predominant form of Aβ in senile plaques, and its accumulation has been associated with increased neurotoxicity.[78] Previous studies showed that some benzofuran derivatives were able to reduce aggregated Aβ in the brain.[25]

Therefore, all synthesized derivatives were screened to assess the structural elements responsible for the inhibitory activity. To properly rank the benzofuran−tacrine hybrids, the inhibitors were screened at a concentration close to the IC_{50} value of the reference compound bis(7)-tacrine, which is 8.4 ± 1.4 μM,[44] i.e., 10 μM, which corresponds to Aβ/inhibitor = 5/1.

DOI: 10.1021/acs.jmedchem.5b01119
J. Med. Chem. 2016, 59, 114−131

An analysis of the results reported in Table 1 for hybrids **1a**–**1l** reveals that independently of the length of the spacer chain, the tacrine–methoxybenzofuran hybrids, i.e., hybrids bearing both the 7-methoxybenzofuran moiety and the 1,2,3,4-tetrahydroacridine unit, exert the highest inhibitory activity, i.e., 40.2% and 42.5% for **1e** and **1k**, respectively. The presence of both moieties seems to be a key feature for the optimal inhibitory activity. Indeed, the removal of the methoxy group, as in **1b** and **1h**, led to significantly less potent inhibitors (inhibition of 13.7% vs 40.2% and 26.2% vs 42.5%, for **1b** vs **1e** and **1h** vs **1k**, respectively). Similarly, 7-methoxybenzofuran hybrids containing a 2,3-dihydro-1*H*-cyclopenta[*b*]quinoline unit or a 7,8,9,10-tetrahydro-6*H*-cyclohepta[*b*]quinoline unit were significantly weaker than the corresponding hybrids bearing a tacrine unit (e.g., **1k** vs **1j** and **1l**). In hybrids from series **2**, the presence of an amino group enhanced the inhibitory potency, which led to hybrids with the highest inhibitory potency. The most potent hybrids were **2b**, **2d**, and **2e**, which showed inhibition between 61.6% and 71.3%. These three compounds were all more potent than the reference compound bis(7)-tacrine, which showed 51% inhibition at the same concentration. Thus, these compounds can definitively be considered strong inhibitors against β-amyloid self-aggregation.

Finally, the presence of two 7-methoxybenzofuran units (series **3**) led to new derivatives with generally higher inhibitory activities compared with hybrids bearing a single 7-methoxybenzofuran unit. For derivatives within series **3**, the benefit of the methoxy substituent on the benzofuran unit seemed to be lost, while the importance of having a 1,2,3,4-tetrahydroacridine unit remained, even if at a lower extent.

Note that the lack of activity in the reference compound tacrine shows that the tetrahydroacridine fragment is unable to inhibit Aβ oligomerization by itself.

Cell Viability Assay on the SH-SY5Y Cell Line. The effects of compound **2e** on cell viability were determined at 3, 10, and 30 μM in parallel with tacrine. The experimental data showed that exposing SH-SY5Y cells for 48 h to **2e** or tacrine at either 3 or 10 μM did not significantly reduce cell viability (Figure 4). However, at 30 μM, both **2e** and tacrine significantly affected viability ($p < 0.01$), and the cytotoxic effect was higher for **2e** than tacrine (63.0 ± 20.1% vs 33.8 ± 5.1%). In general, the cell toxicity profile of **2e** roughly matches that of tacrine, with higher cytotoxicity at the highest tested concentration (30 μM). Representative analogues from series **1** (**1h**) and **3** (**3c**) were also assayed. Derivatives **1k** and **3c** were significantly more cytotoxic than **2e** (Supporting Information, Figure S5), which therefore confirmed that **2e** was the best candidate for further investigation.

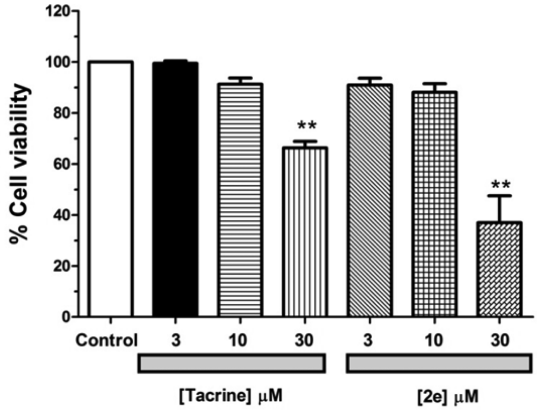

Figure 4. Cell viability, measured as the reduction of MTT, in SH-SY5Y cells exposed for 48 h with increasing concentrations of **2e** or tacrine. Data correspond to the mean ± SEM of four different experiments performed in triplicate. $^{**}p < 0.01$, in comparison with the basal condition in the absence of the tested compound.

Behavioral Studies. Cognition-improving potency is of utmost importance for anti-AD agents. Given the interesting multipotent activity profile of **2e**, its ability to ameliorate scopolamine-induced cognition impairment in ICR mice was investigated in a behavioral study using a Morris water maze test.[79] Scopolamine-induced cognition-impaired adult mice were used as an animal model to measure the cognitive improvement effects of **2e** compared with tacrine (in equimolar doses). Tacrine and **2e** (20 μmol/kg body weight) were orally administered to the ICR mice 30 min before intraperitoneal (ip) administration of scopolamine (1 mg/kg) or saline solution for 10 consecutive days to adapt the apparatus. The test included 5 days of learning and memory training and a probe trial on the sixth day. Figure 5 shows the mean values of

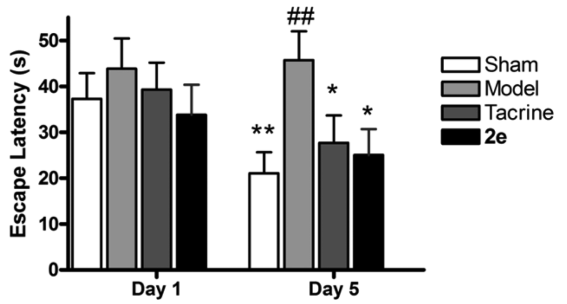

Figure 5. Effects of oral administration of **2e** (20 μmol/kg) and tacrine (20 μmol/kg) on scopolamine-induced memory impairment in ICR mice evaluated by the Morris water maze test. Data are presented as the mean ± SEM (n = 9–10; $^{*}p < 0.05$, $^{**}p < 0.01$ *vs sham group*; $^{\#\#}p < 0.01$, *vs scopolamine group*).

the escape latencies to the hidden platform at day 1 and day 5 (the mean escape latency values for each training day are provided as Supporting Information, Table S3 and Figure S6). Sham-operated mice exhibited a reduction of mean escape latency from 37.4 to 21.1 s ($^{**}p < 0.01$) over the course of five training days. Compared with the sham group, the **2e**-treated group had similar but better performance than the tacrine-treated group, displaying a reduction of mean escape latency from 33.8 to 22.1 s ($^{*}p < 0.05$), whereas the tacrine group showed a reduction from 39.3 to 27.7 s ($^{*}p < 0.05$).

Furthermore, in the probe trial on day 6, the administration of **2e** significantly improved the overall target quadrant preference (36.25%, $^{**}p < 0.01$) compared with the tacrine-treated group (32.5%, $^{*}p < 0.05$) (Figure 6 and Supporting Information, Table S4). These results indicated that **2e** considerably ameliorated the cognition impairment of the treated mice and also suggested that **2e** may penetrate the blood–brain barrier and target the central nervous system.

Hepatotoxicity Studies. The possible drug-induced hepatotoxicity associated with the presence of the tetrahydroacridine nucleus in **2e** was investigated. The serious hepatotoxicity associated with tacrine intake has been the primary limitation for its clinical use. Approximately half of patients treated with tacrine showed liver enzyme abnormalities.[11] Compound **2e**, tacrine, and bis(7)-tacrine were assayed at equimolar doses in

DOI: 10.1021/acs.jmedchem.5b01119
J. Med. Chem. 2016, 59, 114–131

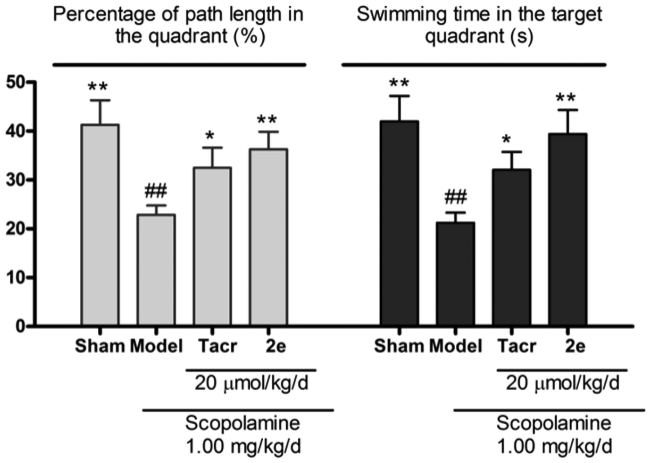

Figure 6. Effects of oral administration of **2e** and tacrine on spatial bias (% of total distance swum in the training quadrant during the spatial probe trial). Data are presented as the mean ± SEM (n = 9−10; *p < 0.05, **p < 0.01, *vs sham group*; ##p < 0.01, *vs scopolamine group*). Tacr stands for tacrine.

adult mice, and their toxicity profiles were compared. Heparinized serum was collected 8, 22, and 36 h after the administration of tacrine, bis(7)-tacrine, and **2e**, and the levels of aspartate aminotranferase (ASAT) and alanine aminotranferase (ALT) were evaluated (Table 3). The serum levels of ASAT and ALT are directly related to the extent of the liver damage.[80] Indeed, clinical evidence has shown that tacrine therapy is associated with an elevation in serum aminotransferase activity in almost half of patients in addition to acute liver injury.[11] In agreement with that clinical evidence, significantly elevated ALT and ASAT activities were detected in tacrine-treated mice, indicating that liver was affected during the acute exposure. Specifically, 8 h after tacrine administration, a statistically significant increase in both ALT (1.6-fold, $p \leq 0.001$) and ASAT (1.5-fold, $p \leq 0.05$) was observed. On the other hand, when **2e** was administered, only a slight increase in ALT (1.16-fold, not statistically significant) and ASAT (1.22-fold, not statistically significant) was observed. In general, both bis(7)-tacrine and **2e** showed a significantly lower hepatotoxicity than tacrine when tested at equimolar doses, and **2e** showed the highest safety among the three tested compounds.

CONCLUSIONS

Developing a single molecule able to strongly interact with structurally distinct targets is not an easy task, even using computer-aided drug design.[81] For the series of hybrids developed and characterized in the present work, the results from in vitro and in vivo tests confirmed that they have an interesting MTDL profile: they are able to reduce the hydrolytic activity of *h*AChE, potentially prevent amyloid production through the inhibition of *h*BACE-1 activity, and interfere with amyloid aggregation. In particular, the most interesting derivative within this series, the hybrid **2e**, showed an inhibitory potency against human AChE in the subnanomolar range, a mixed-type mechanism of inhibition, and the ability to partially inhibit AChE-induced Aβ fibril formation. Moreover, it displayed a significant inhibition of amyloid self-aggregation (at [I]/Aβ = 1/5) and a good inhibitory potency (low micromolar range) against *h*BACE-1.

The X-ray crystal structure of **2e** in complex with *Tc*AChE, besides highlighting the mode of interaction and providing the molecular basis for interpreting the biological data, provided some general considerations for future AChEI design. Indeed, the conformational plasticity of the functional residues lining the active-site gorge of AChE has significant implications for structure-based drug design, as it has been observed in the *Tc*AChE−**2e** complex as well as in other complexes.[54,56−58] The outcomes of the structural study highlight the limitations of designing new inhibitors using the native enzyme structure as a rigid template, and they suggest that small-to-large-scale conformational heterogeneity should be taken into account. An additional and important outcome of this structural study is the possible advantage of choosing an appropriate ensemble of protein structures in docking-based virtual screening rather than using a single protein conformation.

Furthermore, ICR male mice treated with scopolamine (1 mg/kg/day) showed significantly ameliorated memory performance in a Morris water maze test when **2e** was administered.

Finally, results from hepatotoxicity studies demonstrated evidence that modification of the parent scaffold of tacrine may lead to safer tacrine derivatives. Levels of serum biomarkers for acute liver toxicity confirmed that **2e** was significantly safer than tacrine. The advantageous biological properties and safety profile of hybrid **2e**, along with its likely ability to reach the CNS, make it an interesting new lead compound. Thus, **2e** can be used for further studies to help understand the structural requirements for an optimal MTDL for AD treatment.

The potential in vivo relevance of the multiple activities shown in the in vitro assays deserves a final comment. For example, the concentration required to inhibit amyloid aggregation is much higher (μM range) than that necessary to inhibit *h*AChE (in the nanomolar/subnanomolar range). Nevertheless, to properly compare activities, data from each in vitro assay need to first be "normalized" on the basis of the physiological/pathological levels of the molecular target. In fact, a high concentration of amyloid (50 μM) is required in the in vitro assay to aggregate in a suitable time frame, while in vivo

Table 3. ALT and ASAT Activity after the Administration of 2e and Reference Compounds Tacrine (30 mg/kg) and bis(7)-tacrine (30 mg/kg)[a]

	ALT (U/L)			ASAT (U/L)		
	8 h	22 h	36 h	8 h	22 h	36 h
control	38.8 ± 10.1	40.1 ± 9.9	38.1 ± 8.2	113.3 ± 30.0	113.9 ± 31.1	110.6 ± 23.1
tacrine	62.7 ± 13.9***	65.7 ± 20.3**	55.4 ± 16.3*	170.4 ± 57.6*	151.6 ± 32.7*	138.1 ± 38.6
bis(7)-tacrine	49.9 ± 13.0	50.8 ± 9.1*	44.8 ± 10.5	142.4 ± 23.5*	132.7 ± 6.0	113.9 ± 4.5
2e	45.1 ± 7.9	48.2 ± 18.7	42.0 ± 5.1	138.3 ± 21.6	134.5 ± 33.8	114.7 ± 16.9

[a]Values are expressed as the mean ± SD (n = 8−9; t test, compared with a no-treatment control group after the same amounts of time, *$p \leq 0.05$, **$p \leq 0.01$, ***$p \leq 0.001$).

DOI: 10.1021/acs.jmedchem.5b01119
J. Med. Chem. 2016, 59, 114−131

Aβ concentration is estimated to be in the nanomolar/subnanomolar range.[82] Therefore, because the hybrids were active at a concentration five times lower than that of Aβ, it seems plausible that, provided a suitable pharmacokinetic and proper BBB crossing, the most potent tacrine−benzofuran hybrids may exert their inhibitory activity at nanomolar concentrations.

EXPERIMENTAL SECTION

Chemistry. All chemicals (reagent grade) were purchased from Sinopharm Chemical Reagent Co. Ltd. (Shanghai, China). Reference compound bis(7)-tacrine was synthesized following the previously reported protocol.[83] Intermediate compounds **4a−4e**[18,35−37] and **5a−5d**[38−40] were also synthesized following previously reported protocols. Reactions were followed by thin-layer chromatography (TLC) on silica gel GF_{254} plates (Qingdao Haiyang Chemical Plant, Qingdao, China), and the spots were visualized using a UV lamp (λ = 254 nm). Chromatographic separations were performed on silica gel columns (90−150 μm; Qingdao Marine Chemical Inc., Qingdao, Shandong, China) by flash chromatography. Melting points were measured on an XT-4 micromelting point instrument (Beijing Tech Instrument Corp., Beijing, China) and were uncorrected. IR (KBr-disc) spectra were recorded by Bruker Tensor 27 spectrometer (Bruker Corp., Billerica, MA, USA). ^{1}H NMR spectra (300 or 500 MHz) and ^{13}C NMR (75 or 125 MHz) were acquired on a Bruker ACF-300 or ACF-500 spectrometer (Bruker Corp., Billerica, MA, USA) at 25 °C and referenced to tetramethylsilane (TMS). Chemical shifts were reported in ppm (δ) using the residue solvent line as the internal standard. Splitting patterns are designated as: s, singlet; br s, broad singlet; d, doublet; dd, doublet of doublets; t, triplet; dt, doublet of triplets; q, quartet; and m, multiplet. The identity of the final compounds was confirmed by acquiring mass spectra on an Agilent 1100 series LC/MSD high performance ion trap mass spectrometer (Agilent Technologies, Santa Clara, CA, USA) and a Mariner ESI-TOF spectrometer (Applied Biosystems, Foster, CA, USA). Compound purities were evaluated by reverse-phase chromatography using a Shimadzu Shim-Pack VP-ODS (150 mm × 4.6 mm i.d., 5 μm particle size) column (Shimadzu Corp., Kyoto, Japan) and DAD detection. Satisfactory chromatographic analyses were obtained for all new compounds, confirming >95% purity (see Supporting Information).

Synthesis of 1a−1l. *General Procedure I.* A mixture of benzofuran-2-carboxylic acid (**5a**) or 7-methoxy-1-benzofuran-2-carboxylic acid (**5b**) (2 mmol) and 1,1′-carbonyldiimidazole (2.05 mmol) in 25 mL of anhydrous THF was stirred for 3 h at rt before the dropwise addition of a 5 mL solution of **4a−4f** (2 mmol) in anhydrous THF. The final mixtures were stirred for 4 h. The reaction mixture was washed with saturated aqueous solution of sodium chloride (3 × 25 mL) and extracted with CH_2Cl_2 (3 × 25 mL). The combined organic layers were dried over anhydrous Na_2SO_4 and evaporated under vacuum. Purification of the crude product was achieved by column chromatography (CH_2Cl_2:MeOH:triethylamine = 30:1:0.5, *v:v:v*) to afford **1a−1l**.

*N-(6-((2,3-Dihydro-1H-cyclopenta[b]quinolin-9-yl)amino)hexyl)-benzofuran-2-carboxamide (**1a**).* Compound **1a** was prepared according to the general procedure I, white solid, yield 65%, mp 118−120 °C. ^{1}H NMR ($CDCl_3$, 500 MHz): δ ppm 7.96 (d, 1H, *J* = 8.3 Hz), 7.81 (d, 1H, *J* = 8.2 Hz), 7.79 (d, 1H, *J* = 7.8 Hz), 7.58 (dt, 1H, *J* = 8.4, 1.2 Hz), 7.50 (dt, 1H, *J* = 8.4, 0.7 Hz), 7.48 (s, 1H), 7.44 (dt, 1H, *J* = 7.2, 1.2 Hz), 7.40 (dt, 1H, *J* = 8.2, 1.2 Hz), 7.32 (dt, 1H, *J* = 8.0, 0.9 Hz), 6.69 (s, 1H), 4.85 (s, 1H), 3.64 (q, 2H, *J* = 6.9 Hz), 3.53 (q, 2H, *J* = 6.8 Hz), 3.22 (t, 2H, *J* = 7.1 Hz), 3.10 (t, 2H, *J* = 7.8 Hz), 2.15 (t, 2H, *J* = 7.5 Hz), 1.75−1.68 (m, 4H), 1.57−1.46 (m, 4H). ^{13}C NMR ($CDCl_3$, 75 MHz): δ ppm 168.3, 159.1, 154.8, 148.9, 147.9, 146.9, 128.8, 128.7, 127.8, 127.0, 124.2, 123.9, 122.9, 120.0, 119.0, 114.1, 111.8, 110.4, 53.1, 39.2, 34.9, 31.2, 31.0, 29.8, 26.6, 26.4, 23.4. IR (KBr): ν 3359, 2927, 2854, 1657, 1573, 1546, 1305, 748 cm^{-1}. MS (*m/z*): 428.2 ([M + H]$^+$). HRMS (*m/z*): calcd for $C_{27}H_{30}N_3O_2$ [M + H]$^+$, 428.2333; found, 428.2347.

*N-((1,2,3,4-Tetrahydroacridin-9-ylamino)methyl)benzofuran-2-carboxamide (**1b**).* Compound **1b** was prepared according to the general procedure I, yellow oil, yield 78%. ^{1}H NMR ($CDCl_3$, 300 MHz): δ ppm 7.98−7.93 (m, 2H), 7.64 (d, 1H, *J* = 7.7 Hz), 7.55−7.50 (m, 1H), 7.46 (br s, 1H), 7.46−7.44 (m, 1H), 7.40−7.24 (m, 3H), 6.86 (s, 1H), 3.52−3.43 (m, 4H), 3.06 (br s, 2H), 2.67 (br s, 2H), 1.88 (br s, 4H), 1.67−1.62 (m, 4H), 1.44−1.43 (m, 4H). ^{13}C NMR ($CDCl_3$, 75 MHz): δ ppm 167.5, 158.9, 154.5, 151.0, 148.7, 146.6, 128.4, 127.8, 127.5, 126.7, 123.6, 123.5, 122.8, 122.5, 119.7, 115.4, 114.5, 110.1, 49.1, 39.2, 33.4, 31.4, 29.4, 26.5, 26.4, 24.6, 22.8, 22.5. IR (KBr): ν 3366, 2929, 2856, 1653, 1581, 1563, 1298, 749 cm^{-1}. MS (*m/z*): 442.1 ([M + H]$^+$). HRMS (*m/z*): calcd for $C_{28}H_{32}N_3O_2$ [M + H]$^+$, 442.2489; found, 442.2493.

*N-(6-((7,8,9,10-Tetrahydro-6H-cyclohepta[b]quinolin-11-yl)-amino)hexyl)benzofuran-2-carboxamide (**1c**).* Compound **1c** was prepared according to the general procedure I, yellow oil, yield 65%. ^{1}H NMR ($CDCl_3$, 500 MHz): δ ppm 7.95 (d, 1H, *J* = 8.3 Hz), 7.89 (d, 1H, *J* = 8.3 Hz), 7.66 (d, 1H, *J* = 7.8 Hz), 7.55 (dt, 1H, *J* = 6.9, 1.2 Hz), 7.47 (t, 1H, *J* = 8.3 Hz), 7.45 (s, 1H), 7.42−7.38 (m, 2H), 7.30−7.26 (m, 1H), 6.68 (br s, 1H), 3.89 (br s, 1H), 3.47 (q, 2H, *J* = 6.9 Hz), 3.27 (q, 2H, *J* = 7.2 Hz), 3.16 (t, 2H, *J* = 5.7 Hz), 2.90 (t, 2H, *J* = 5.5 Hz), 1.87−1.85 (m, 2H), 1.80−1.78 (m, 2H), 1.74−1.63 (m, 2H), 1.49−1.43 (m, 4H), 1.31−1.22 (m, 4H). ^{13}C NMR ($CDCl_3$, 125 MHz): δ ppm 164.9, 159.1, 154.8, 150.3, 148.9, 146.1, 128.6, 127.8, 126.9, 124.9, 123.8, 122.8, 122.1, 118.9, 118.7, 115.2, 111.8, 110.4, 50.5, 39.6, 39.3, 32.0, 31.4, 29.7, 28.3, 27.8, 26.9, 26.8, 26.8. IR (KBr): ν 3448, 2925, 2853, 1646, 1589, 1569, 1300, 750 cm^{-1}. MS (*m/z*): 456.3 ([M + H]$^+$). HRMS (*m/z*): calcd for $C_{29}H_{34}N_3O_2$ [M + H]$^+$, 456.2646; found, 456.2655.

*N-(6-((2,3-Dihydro-1H-cyclopenta[b]quinolin-9-yl)amino)hexyl)-7-methoxybenzofuran-2-carboxamide (**1d**).* Compound **1d** was prepared according to the general procedure I, white solid, yield 68%, mp 120−123 °C. ^{1}H NMR ($CDCl_3$, 300 MHz): δ ppm 7.97 (d, 1H, *J* = 8.3 Hz), 7.86 (d, 1H, *J* = 8.3 Hz), 7.56 (t, 1H, *J* = 7.5 Hz), 7.45 (s, 1H), 7.38 (t, 1H, *J* = 8.3 Hz), 7.24−7.18 (m, 2H), 6.91 (d, 1H, *J* = 7.6 Hz), 6.79 (br s, 1H), 5.11 (br s, 1H), 4.01 (s, 3H), 3.62 (q, 2H, *J* = 7.2 Hz), 3.49 (q, 2H, *J* = 6.8 Hz), 3.19 (t, 2H, *J* = 7.2 Hz), 3.09 (t, 2H, *J* = 7.7 Hz), 2.13 (t, 2H, *J* = 7.5 Hz), 1.70−1.65 (m, 4H), 1.50−1.44 (m, 4H). ^{13}C NMR ($CDCl_3$, 75 MHz): δ ppm 167.5, 159.0, 149.2, 147.6, 146.7, 145.6, 144.4, 129.4, 128. 9, 127.9, 124.5, 124.4, 124.2, 120.3, 114.9, 113.8, 110.9, 108.4, 56.1, 45.4, 39.1, 34.5, 31.2, 31.1, 29.7, 26.5, 26.2, 23.3. IR (KBr): ν 3355, 2925, 2853, 1658, 1574, 1560, 1301, 751 cm^{-1}. MS (*m/z*): 458.2 ([M + H]$^+$). HRMS (*m/z*): calcd for $C_{28}H_{32}N_3O_3$ [M + H]$^+$, 458.2438; found, 458.2454.

*7-Methoxy-N-(6-((1,2,3,4-tetrahydroacridin-9-yl)amino)hexyl)-benzofuran-2-carboxamide (**1e**).* Compound **1e** was prepared according to the general procedure I, yellow oil, yield 70%. ^{1}H NMR ($CDCl_3$, 300 MHz): δ ppm 7.96 (dd, 1H, *J* = 8.5, 0.8 Hz), 7.91 (dd, 1H, *J* = 8.5, 0.7 Hz), 7.54 (dt, 1H, *J* = 8.2, 1.3 Hz), 7.45 (s, 1H), 7.34 (dt, 1H, *J* = 8.3, 1.2 Hz), 7.25−7.16 (m, 2H), 6.88 (dd, 1H, *J* = 7.4, 1.5 Hz), 6.81 (br s, 1H), 3.98 (br s, 1H), 3.98 (s, 3H), 3.48−3.41 (m, 4H), 3.05 (br s, 2H), 2.70 (br s, 2H), 1.91−1.89 (m, 4H), 1.67−1.60 (m, 4H), 1.43−1.40 (m, 4H). ^{13}C NMR ($CDCl_3$, 75 MHz): δ ppm 167.5, 158.9, 158.4, 151.0, 149.2, 145.6, 144.3, 129.5, 128.6, 128.5, 124.5, 123.8, 123.0, 120.3, 116.0, 114.9, 110.9, 108.3, 56.1, 49.5, 39.3, 31.8, 30.1, 29.8, 26.7, 26.6, 24.9, 23.2, 22.9. IR (KBr): ν 3421, 2933, 2857, 1652, 1590, 1491, 1316, 763 cm^{-1}. MS (*m/z*): 472.3 ([M + H]$^+$). HRMS (*m/z*): calcd for $C_{29}H_{34}N_3O_3$ [M + H]$^+$, 472.2595; found, 472.2617.

*7-Methoxy-N-(6-((7,8,9,10-tetrahydro-6H-cyclohepta[b]quinolin-11-yl)amino)hexyl)benzofuran-2-carboxamide (**1f**).* Compound **1f** was prepared according to the general procedure I, yellow solid, yield 62%, mp 75−78 °C. ^{1}H NMR ($CDCl_3$, 300 MHz): δ ppm 7.95 (d, 1H, *J* = 8.3 Hz), 7.90 (d, 1H, *J* = 8.3 Hz), 7.56 (t, 1H, *J* = 8.0 Hz), 7.45 (s, 1H), 7.40 (t, 1H, *J* = 8.1 Hz), 7.27−7.17 (m, 2H), 6.89 (d, 1H, *J* = 7.3 Hz), 6.79 (br s, 1H), 3.99 (s, 3H), 3.46 (q, 2H, *J* = 6.7 Hz), 3.27 (t, 2H, *J* = 7.1 Hz), 3.19−3.15 (m, 2H); 2.93−2.90 (m, 2H), 1.85−1.63 (m, 10H), 1.44−1.43 (m, 4H). ^{13}C NMR ($CDCl_3$, 125 MHz): δ ppm 165.3, 158.9, 150.0, 149.2, 146.6, 145.6, 144.3, 129.4, 129.0, 128.4, 124.9, 124.5, 124.0, 122.2, 122.0, 114.9, 110.8, 108.3, 56.1, 50.7, 39.9,

DOI: 10.1021/acs.jmedchem.5b01119
J. Med. Chem. 2016, 59, 114−131

39.3, 32.1, 31.5, 29.7, 28.4, 27.8, 26.9, 26.8, 26.8. IR (KBr): ν 3391, 2926, 2854, 1655, 1590, 1566, 1315, 758 cm^{-1}. MS (m/z): 486 $[M + H]^+$. HRMS (m/z): calcd for $C_{30}H_{36}N_3O_3$ $[M + H]^+$, 486.2751; found, 486.2769.

*N-(7-((2,3-Dihydro-1H-cyclopenta[b]quinolin-9-yl)amino)heptyl)-benzofuran-2-carboxamide (**1g**).* Compound **1g** was prepared according to the general procedure I, yellow solid, yield 68%, mp 80−83 °C. ^1H NMR ($CDCl_3$, 500 MHz): δ ppm 7.91 (d, 1H, J = 8.4 Hz), 7.74 (d, 1H, J = 8.3 Hz), 7.65 (d, 1H, J = 7.8 Hz), 7.54−7.51 (m, 1H), 7.47−7.45 (m, 1H), 7.45 (s, 1H), 7.39 (dd, 1H, J = 7.3, 1.0 Hz), 7.35−7.32 (m, 1H), 7.29−7.26 (m, 1H), 6.74 (br s, 1H), 4.71 (br s, 1H), 3.57 (q, 2H, J = 6.8 Hz), 3.47 (q, 2H, J = 6.7 Hz), 3.19−3.13 (m, 2 H), 3.05−3.02 (m, 2H), 2.16−2.08 (m, 2H), 1.66−1.62 (m, 4H), 1.47−1.41 (m, 6H). ^{13}C NMR ($CDCl_3$, 125 MHz): δ ppm 168.5, 158.9, 154.6, 148.8, 148.2, 146.4, 128.9, 128.1, 126.7, 123.8, 123.6, 12 2.6, 122.1, 119.7, 118.8, 114.0, 111.6, 110.2, 45.6, 39.2, 34.9, 31.1, 30.8, 29.5, 28.9, 26.7, 26.5, 23.2. IR (KBr): ν 3362, 2927, 2852, 1656, 1574, 1546, 1302, 749 cm^{-1}. MS (m/z): 442.3 $[M + H]^+$. HRMS (m/z): calcd for $C_{28}H_{32}N_3O_2$ $[M + H]^+$, 442.2489; found, 442.2476.

*N-(7-((1,2,3,4-Tetrahydroacridin-9-yl)amino)heptyl)benzofuran-2-carboxamide (**1h**).* Compound **1h** was prepared according to the general procedure I, yellow oil, yield 48%. ^1H NMR ($CDCl_3$, 300 MHz): δ ppm 7.97−7.91 (m, 2H), 7.65 (d, 1H, J = 8.0 Hz), 7.56−7.48 (m, 2H), 7.46 (s, 1H), 7.42−7.25 (m, 3H), 6.76 (s, 1H), 3.51−3.43 (m, 4H), 3.06 (br s, 2H), 2.69 (br s, 2H), 1.91−1.89 (m, 4H), 1.66−1.60 (m, 4H), 1.39 (br s, 6H). ^{13}C NMR ($CDCl_3$, 75 MHz): δ ppm 167.7, 159.1, 154.9, 153.4, 148.7, 146.7, 128.7, 127.8, 127.0, 124.8, 124.6, 123.9, 123.7, 122.9, 118.1, 113.3, 111.8, 110.3, 49.1, 39.5, 33.3, 31.5, 31.2, 29.7, 28.9, 26.8, 24.3, 22.6, 21.8. IR (KBr): ν 3424, 2930, 2856, 1644, 1591.9, 1524, 1299, 751 cm^{-1}. MS (m/z): 456.1 ($[M + H]^+$). HRMS (m/z): calcd for $C_{29}H_{34}N_3O_2$ $[M + H]^+$, 456.2646; found, 456.2630.

*N-(7-(7,8,9,10-Tetrahydro-6H-cyclohepta[b]quinolin-11-ylamino)heptyl)benzofuran-2-carboxamide (**1i**).* Compound **1i** was prepared according to the general procedure I, pale-brown oil, yield 68%. ^1H NMR ($CDCl_3$, 500 MHz): δ ppm 8.44 (d, 1H, J = 7.2 Hz), 8.12 (d, 1H, J = 8.2 Hz), 7.65 (d, 1H, J = 7.7 Hz), 7.62 (t, 1H, J = 7.7 Hz), 7.49−7.43 (m, 2H), 7.46 (s, 1H), 7.40 (t, 1H, J = 7.5 Hz), 7.31−7.29 (m, 1H), 6.79 (br s, 1H), 5.30 (s, 1H), 3.63 (br s, 2H), 3.47−3.46 (m, 2H), 3.38 (br s, 2H), 2.88 (br s, 2H), 1.87−1.71 (m, 4H), 1.71−1.63 (m, 2H), 1.40−1.33 (m, 6H), 1.26−1.20 (m, 4H). ^{13}C NMR ($CDCl_3$, 125 MHz): δ ppm 164.0, 158.9, 154.7, 151.2, 148.8, 144.5, 129.2, 127.7, 127.2, 126.8, 125.1, 123.7, 122.7, 122.3, 122.0, 121.0, 111.7, 110.3, 50.3, 39.3, 38.3, 31.8, 31.4, 29.7, 29.4, 28.9, 28.0, 27.5, 26.8, 26.0. IR (KBr): ν 3424, 2924, 2851, 1640, 1584, 1298, 748 cm^{-1}. MS (m/z): 470.3 ($[M + H]^+$). HRMS (m/z): calcd for $C_{29}H_{36}N_3O_2$ $[M + H]^+$, 470.2802; found, 470.2798.

*N-(7-(2,3-Dihydro-1H-cyclopenta[b]quinolin-9-ylamino)heptyl)-7-methoxybenzofuran-2-carboxamide (**1j**).* Compound **1j** was prepared according to the general procedure I, yellow solid, yield 72%, mp 127−129 °C. ^1H NMR ($CDCl_3$, 500 MHz): δ ppm 7.95 (d, 1H, J = 8.3 Hz), 7.79 (d, 1H, J = 8.4 Hz), 7. 55 (t, 1H, J = 7.4 Hz), 7.45 (s, 1H), 7.35 (t, 1H, J = 7.6 Hz), 7.24−7.19 (m, 2H), 6.90 (d, 1H, J = 7.6 Hz), 6.75 (br s, 1H), 5.04 (br s, 1H), 4.01 (s, 3H), 3.62 (t, 2H, J = 7.0 Hz), 3.46 (q, 2H, J = 6.8 Hz), 3.19 (t, 2H, J = 7.2 Hz), 3.09 (t, 2H, J = 7.8 Hz), 2.14 (q, 2H, J = 6.8 Hz), 1.69−1.62 (m, 4H), 1.41−1.34 (m, 6H). ^{13}C NMR ($CDCl_3$, 125 MHz): δ ppm 167.6, 158.7, 149.0, 147.1, 146.9, 145.4, 144.1, 129.2, 128.6, 128.0, 124.3, 124.1, 120.0, 118.6, 114.7, 113.7, 110.7, 108.1, 55.9, 45.5, 39.2, 34.5, 31.1, 30.9, 29.5, 28.9, 26.7, 26.6, 23.1. IR (KBr): ν 3356, 2925, 2851, 1657, 1573, 1458, 1308, 759 cm^{-1}. MS (m/z): 472.3 ($[M + H]^+$). HRMS (m/z): calcd for $C_{29}H_{34}N_3O_3$ $[M + H]^+$, 472.2595; found, 472.2577.

*7-Methoxy-N-(7-((1,2,3,4-tetrahydroacridin-9-yl)amino)heptyl)-benzofuran-2-carboxamide (**1k**).* Compound **1k** was prepared according to the general procedure I, yellow oil, yield 67%. ^1H NMR ($CDCl_3$, 300 MHz): δ ppm 7.98 (dd, 1H, J = 8.6, 0.8 Hz), 7.91 (dd, 1H, J = 8.5, 0.7 Hz), 7.55 (dt, 1H, J = 8.2, 1.3 Hz), 7.45 (s, 1H). 7.34 (dt, 1H, J = 8.3, 1.2 Hz), 7.25−7.16 (m, 2H), 6.88 (dd, 1H, J = 7.4, 1.5 Hz), 6.77 (br s, 1H), 4.12 (br s, 1H), 4.01 (s, 3H), 3.54−3.42 (m, 4H), 3.08 (br s, 2H), 2.69 (br s, 2H), 1.93−1.89 (m, 4H), 1.68−1.60 (m, 4H), 1.39−1.32 (m, 6H). ^{13}C NMR ($CDCl_3$, 75 MHz): δ ppm 167.5, 159.0, 149.2, 147.3, 145.6, 144.3, 139.8, 131.4, 129.2, 128.8, 124.9, 124.6, 124.0, 122.2, 119.2, 114.9, 110.8, 108.4, 56.1, 49.0, 39.3, 31.3, 30.1, 29.8, 29.7, 28.9, 26.7, 24.0, 22.1, 21.0. IR (KBr): ν 3423, 2931, 2856, 1650, 1592, 1491, 1315, 761 cm^{-1}. MS (m/z): 486.1 ($[M + H]^+$). HRMS (m/z): calcd for $C_{30}H_{36}N_3O_2$ $[M + H]^+$, 486.2751; found, 486.2729.

*N-(7-(7,8,9,10-Tetrahydro-6H-cyclohepta[b]quinolin-11-ylamino)heptyl)-7-methoxybenzofuran-2-carboxamide (**1l**).* Compound **1l** was prepared according to the general procedure I, yellow oil, yield 75%. ^1H NMR ($CDCl_3$, 300 MHz): δ ppm 8.48 (d, 1H, J = 8.4 Hz), 8.27 (d, 1H, J = 8.6 Hz), 7.61 (t, 1H, J = 7.5 Hz), 7.45−7.42 (m, 2H), 7.45 (br s, 1H), 7.24−7.16 (m, 2H), 6.94−6.87 (m, 2H), 6.74 (s, 1H), 3.99 (s, 1H), 3.73 (t, 2H, J = 6.8 Hz), 3.46−3.39 (m, 4H), 2.88−2.85 (m, 2H), 1.81−1.74 (m, 6H), 1.70−1.59 (m, 4H), 1.34−1.27 (m, 6H). ^{13}C NMR ($CDCl_3$, 75 MHz): δ ppm 167.8, 158.8, 149.0, 147.5, 145.4, 144.1, 137.6, 129.3, 128.8, 125.9, 124.3, 124.0, 123.3, 121.0, 119.5, 114.6, 110.5, 108.2, 55.9, 48.9, 38.6, 39.1, 33.6, 31.1, 30.9, 29.6, 29.4, 28.6, 27.1, 25.7, 22.4. IR (KBr): ν 3423, 2924, 2850, 1640, 1561, 1540, 1289, 749 cm^{-1}. MS (m/z): 500.3 ($[M + H]^+$). HRMS (m/z): calcd for $C_{31}H_{38}N_3O_3$ $[M + H]^+$, 500.2908; found, 500.2886.

Synthesis of 2a−2f and 3a−3h. *General Procedure II.* To a mixture of **4a−4f** (1 mmol) and 2-(bromomethyl)benzofuran (**5c**) or 2-(bromomethyl)-7-methoxybenzofuran (**5d**) (1 mmol) in 20 mL of CH_2Cl_2 was added with K_2CO_3 (0.8 g) and KI (0.08g), and the reaction mixture was stirred for 3 days at rt until the completion monitored by TLC. Then 200 mL of CH_2Cl_2 were added to the mixture and then washed with a saturated aqueous solution of sodium chloride. The organic layer was dried over anhydrous Na_2SO_4 and evaporated under vacuum. Purification was achieved by column chromatography (CH_2Cl_2:EtOAc:MeOH = 30:1:1, v:v:v) to afford **2a−2f** and **3a−3h.**

*N^1-(Benzofuran-2-ylmethyl)-N^6-(2,3-dihydro-1H-cyclopenta[b]-quinolin-9-yl)hexane-1,6-diamine (**2a**).* Compound **2a** was prepared according to the general procedure II, yellow oil, yield 30%. ^1H NMR ($CDCl_3$, 300 MHz): δ ppm 8.25 (d, 1H, J = 8.3 Hz), 7.93 (d, 1H, J = 8.0 Hz), 7.55−7.53 (m, 2H), 7.40−7.36 (m, 2H), 7.24−7.17 (m, 2H), 6.79 (s, 1H), 4.10 (s, 2H), 3.55 (t, 2H, J = 7.0 Hz), 3.11 (t, 2H, J = 7.9 Hz), 2.93 (t, 2H, J = 7.0 Hz), 2.81 (t, 2H, J = 6.8 Hz), 2.09−2.02 (m, 2H), 1.67−1.65 (m, 4H), 1.47−1.39 (m, 4H). ^{13}C NMR ($CDCl_3$, 75 MHz): δ ppm 158.7, 157.2, 155.3, 151.3, 147.6, 144.9, 128.7, 128.5, 128.3, 124.9, 123.8, 122.6, 121.9, 120.7, 116.4, 111.2, 105.5, 53.4, 50.6, 47.0, 34.2, 31.4, 30.2, 29.2, 26.9, 26.7, 23.4. IR (KBr): ν 3420, 2930, 2856, 1587, 1490, 1270, 751 cm^{-1}. MS (m/z): 414.1 ($[M + H]^+$). HRMS (m/z): calcd for $C_{27}H_{32}N_3O$ $[M + H]^+$, 414.2540; found, 414.2521.

*N^1-(2,3-Dihydro-1H-cyclopenta[b]quinolin-9-yl)-N^6-((7-methoxybenzofuran-2-yl)methyl)hexane-1,6-diamine (**2b**).* Compound **2b** was prepared according to the general procedure II, yellow solid, yield 27%, mp 82−85 °C. ^1H NMR ($CDCl_3$, 300 MHz): δ ppm 7.90−7.86 (m, 2H), 7.54 (t, 1H, J = 7.6 Hz), 7.35 (t, 1H, J = 7.4 Hz), 7.13−7.11 (m, 2H), 6.79−6.73 (m, 1H), 6.56 (s, 1H), 3.99 (s, 3H), 3.94 (s, 2H), 3.64 (t, 2H, J = 7.1 Hz), 3.13−3.03 (m, 4H), 2.64 (t, 2H, J = 7.0 Hz), 2.17−2.04 (m, 2H), 1.66−1.64 (m, 2H), 1.55−1.48 (m, 2H), 1.41−1.39 (m, 4H). ^{13}C NMR ($CDCl_3$, 75 MHz): δ ppm 156.8, 156.6, 152.1, 145.1, 145.0, 144.1, 128.9, 126.7, 123.9, 123.6, 122.7, 119.7, 114.2, 113.2, 111.6, 106.4, 104.2, 55.7, 49.2, 48.7, 45.6, 34.9, 31.1, 30.8, 29.6, 28.9, 26.7, 23.2. IR (KBr): ν 3422, 2927, 2854, 1581, 1488, 1271, 758 cm^{-1}. MS (m/z): 444.1 ($[M + H]^+$). HRMS (m/z): calcd for $C_{28}H_{34}N_3O_2$ $[M + H]^+$, 444.2789; found, 444.2781.

*N^1-((7-Methoxybenzofuran-2-yl)methyl)-N^6-(1,2,3,4-tetrahydroacridin-9-yl)hexane-1,6-diamine (**2c**).* Compound **2c** was prepared according to the general procedure II, yellow oil, yield 29%. ^1H NMR ($CDCl_3$, 500 MHz): δ ppm 8.05 (d, 1H, J = 8.5 Hz), 7.99 (d, 1H, J = 8.3 Hz), 7.58 (t, 1H, J = 7.1 Hz), 7.36 (t, 1H, J = 7.2 Hz), 7.14−7.10 (m, 2H), 6.76 (dd, 1H, J = 6.3, 2.7 Hz), 6.55 (s, 1H), 3.99 (s, 3H), 3.93 (s, 2H), 3.59−3.56 (m, 2H), 3.12 (s, 2H), 2.65−2.62 (m, 4H), 1.90−1.89 (m, 4H), 1.72−1.66 (m, 2H), 1.55−1.49 (m, 2H), 1.41−1.36 (m, 4H). ^{13}C NMR ($CDCl_3$, 125 MHz): δ ppm 156.8, 156.5,

DOI: 10.1021/acs.jmedchem.5b01119
J. Med. Chem. 2016, 59, 114−131

152.1, 145.1, 145.0, 144.1, 130.1, 129.4, 126.5, 124.0, 123.3, 123.1, 119.0, 114.4, 113.1, 106.0, 104.1, 55.9, 49.1, 48.7, 46.4, 31.5, 29.8, 29.7, 26.9, 26.7, 24.4, 22.7, 22.1. IR (KBr): ν 3419, 2924, 2852, 1583, 1490, 1261, 749 cm^{-1}. MS (m/z): 458.3 ($[M + H]^+$). HRMS (m/z): calcd for $C_{29}H_{35}N_3O_2$ $[M + H]^+$, 458.2749; found, 458.2762.

*N^1-(Benzofuran-2-ylmethyl)-N^7-(2,3-dihydro-1H-cyclopenta[b]-quinolin-9-yl)heptane-1,7-diamine (**2d**).* Compound **2d** was prepared according to the general procedure II, pale-brown oil, yield 28%. ^1H NMR ($CDCl_3$, 300 MHz): δ ppm 7.93 (d, 2H, J = 8.3 Hz), 7.55−7.49 (m, 2H), 7.43 (d, 1H, J = 7.7 Hz), 7.35 (t, 1H, J = 7.5 Hz), 7.23−7.16 (m, 2H), 6.56 (s, 1H), 5.80 (br s, 1H), 3.92 (s, 2H), 3.61 (br s, 2H), 3.11 (q, 4H, J = 7.1 Hz), 2.65 (t, 2H, J = 7.0 Hz), 2.14−2.09 (m, 2H), 1.67−1.64 (m, 2H), 1.53−1.51 (m, 2H), 1.37−1.30 (m, 6H). ^{13}C NMR ($CDCl_3$, 75 MHz): δ ppm 158.7, 157.5, 155.2, 151.2, 147.8, 144.7, 129.2, 128.4, 126.0, 124.4, 123.7, 122.6, 120.6, 118.2, 113.1, 111.0, 103.8, 49.0, 46.6, 45.3, 33.7, 31.2, 31.0, 29.7, 29.6, 29.1, 27.0, 26.5. IR (KBr): ν 3422, 2926, 2853, 1583, 1492, 1268, 754 cm^{-1}. MS (m/z): 428.7 ($[M + H]^+$). HRMS (m/z): calcd for $C_{28}H_{34}N_3O$ $[M + H]^+$, 428.2696; found, 428.2679.

*N^1-(Benzofuran-2-ylmethyl)-N^7-(1,2,3,4-tetrahydroacridin-9-yl)-heptane-1,7-diamine (**2e**).* Compound **2e** was prepared according to the general procedure II, yellow oil, yield 30%. ^1H NMR ($CDCl_3$, 500 MHz): δ ppm 7.95−7.90 (m, 2H), 7.56−7.50 (m, 2H), 7.44 (d, 1H, J = 8.0 Hz), 7.35−7.32 (m, 1H), 7.25−7.17 (m, 2H), 6.54 (s, 1H), 3.92 (s, 2H), 3.48 (t, 2H, J = 7.2 Hz), 3.06 (br s, 2H), 2.70 (br s, 2H), 2.64 (t, 2H, J = 7.2 Hz), 1.91−1.90 (m, 4H), 1.67−1.61 (m, 2H), 1.51−1.49 (m, 2H), 1.32−1.26 (m, 6H). ^{13}C NMR ($CDCl_3$, 75 MHz): δ ppm 158.6, 157.2, 155.2, 151.0, 147.7, 129.0, 128.7, 128.5, 124.0, 123.8, 123.0, 122.8, 120.9, 120.5, 116.1, 111.3, 103.9, 49.7, 49.4, 47.0, 34.2, 31.9, 30.2, 29.5, 27.4, 27.1, 25.0, 23.3, 23.0. IR (KBr): ν 3418, 2930, 2855, 1581, 1490, 1271, 753 cm^{-1}. MS (m/z): 442.3 ($[M + H]^+$). HRMS (m/z): calcd for $C_{29}H_{36}N_3O$ $[M + H]^+$, 442.2858; found, 442.2868.

*N^1-((7-Methoxybenzofuran-2-yl)methyl)-N^7-(7,8,9,10-tetrahydro-6H-cyclohepta[b]quinolin-11-yl)heptane-1,7-diamine (**2f**).* Compound **2f** was prepared according to the general procedure II, yellow oil, yield 43%. ^1H NMR ($CDCl_3$, 500 MHz): δ ppm 8.29 (br s, 1H), 7.95 (d, 1H, J = 8.5 Hz), 7.64 (t, 1H, J = 7.4 Hz), 7.46 (t, 1H, J = 7.4 Hz), 7.14−7.12 (m, 2H), 6.77 (dd, 2H, J = 6.2, 2.4 Hz), 6.59 (s, 1H), 4.00 (s, 3H), 3.96 (s, 2H), 3.48 (br s, 2H), 3.32 (br s, 2H), 2.88−2.86 (m, 2H), 2.65 (t, 2H, J = 7.1 Hz), 1.89 (br s, 2H), 1.82−1.78 (m, 2H), 1.72−1.69 (m, 4H), 1.51−1.47 (m, 2H), 1.39−1.26 (m, 10H). ^{13}C NMR ($CDCl_3$, 125 MHz): δ ppm 156.8, 156.2, 152.6, 145.2, 145.0, 144.2, 130.1, 128.9, 125.4, 125.3, 123.4, 122.6, 122.5, 122.4, 113.2, 106.1, 104.5, 56. 0, 49.9, 48.8, 46.3, 39.2, 31.6, 31.2, 29.7, 29.5, 29.0, 27.6, 27.0, 26.7, 26.3. IR(KBr): ν 3424, 2923, 2852, 1586, 1494, 1265, 752 cm^{-1}. MS (m/z): 486.3 ($[M + H]^+$). HRMS (m/z): calcd for $C_{31}H_{40}N_3O_2$ $[M + H]^+$, 486.3115; found, 486.3099.

*N^1,N^1-Bis(benzofuran-2-ylmethyl)-N^6-(2,3-dihydro-1H-cyclopenta[b]quinolin-9-yl)hexane-1,6-diamine (**3a**).* Compound **3a** was prepared according to the general procedure II, yellow oil, yield 40%. ^1H NMR ($CDCl_3$, 300 MHz): δ ppm 7.93 (d, 1H, J = 8.3 Hz), 7.71 (d, 1H, J = 8.4 Hz), 7.53 (d, 2H, J = 7.1 Hz), 7.47 (d, 2H, J = 7.8 Hz), 7.41−7.32 (m, 2H), 7.23−7.13 (m, 4H), 6.62 (s, 2H), 4.74 (s, 1H), 3.89 (s, 4H), 3.54 (s, 2H), 3.17 (t, 2H, J = 7.2 Hz), 3.06 (t, 2H, J = 7.8 Hz), 2.60 (t, 2H, J = 7.1 Hz), 2.19−2.06 (m, 2H), 1.63 (s, 4H), 1.40−1.38 (m, 4H). ^{13}C NMR ($CDCl_3$, 75 MHz): δ ppm 158.7, 157.4, 155.4, 151.5, 147.9, 130.0, 128.9, 128.5, 125.0, 124.0, 122.8, 121.0, 120.8, 119.4, 118.0, 111.3, 105.7, 53.4, 50.8, 45.5, 33.4, 31.4, 31.2, 29.8, 27.4, 27.0, 26.6. IR (KBr): ν 3446, 2927, 2854, 1567, 1453, 1252, 752 cm^{-1}. MS (m/z): 544.1 ($[M + H]^+$). HRMS (m/z): calcd for $C_{36}H_{38}N_3O_2$ $[M + H]^+$, 544.2959; found, 544.2940.

*N^1-(2,3-Dihydro-1H-cyclopenta[b]quinolin-9-yl)-N^6,N^6-bis((7-methoxybenzofuran-2-yl)methyl)hexane-1,6-diamine (**3b**).* Compound **3b** was prepared according to the general procedure II, yellow oil, yield 42%. ^1H NMR ($CDCl_3$, 500 MHz): δ ppm 7.96 (d, 1H, J = 8.3 Hz), 7.80 (d, 1H, J = 8.5 Hz), 7.55−7.51 (m, 1H), 7.34 (t, 1H, J = 7.9 Hz), 7.12−7.09 (m, 4H), 6.77−6.73 (m, 2H), 6.63 (s, 2H), 3.98 (s, 6H), 3.90 (s, 4H), 3.57 (t, 2H, J = 7.1 Hz), 3.15−3.08 (m, 4H), 2.61 (t, 2H, J = 7.2 Hz), 2.14−2.08 (m, 2H), 1.75−1.69 (m, 2H), 1.64−1.58 (m, 4H), 1.48−1.43 (m, 2H). ^{13}C NMR ($CDCl_3$, 125 MHz): δ ppm 156.8, 155.7, 152.1, 145.2, 145.0, 144.2, 130.9, 129.1, 128.8, 126.7, 124.3, 123.3, 120.3, 118.2, 113.1, 106.1, 105.5, 56.0, 53.1, 50.6, 45.4, 34.9, 31.2, 30.6, 29.7, 27.3, 26.8, 26.4, 26.0. IR (KBr): ν 3444, 2927, 2855, 1567, 1493.0, 1270, 758 cm^{-1}. MS (m/z): 604.4 ($[M + H]^+$). HRMS (m/z): calcd for $C_{38}H_{42}N_3O_4$ $[M + H]^+$, 604.3170; found, 604.3146.

*N^1,N^1-Bis(7-methoxybenzofuran-2-yl)methyl)-N^6-(1,2,3,4-tetrahydroacridin-9-yl)hexane-1,6-diamine (**3c**).* Compound **3c** was prepared according to the general procedure II, yellow oil, yield 40%. ^1H NMR ($CDCl_3$, 300 MHz): δ ppm 7.95 (d, 2H, J = 8.9 Hz), 7.55 (t, 1H, J = 7.2 Hz), 7.32 (t, 1H, J = 7.2 Hz), 7.12−7.03 (m, 4H), 6.78−6.69 (m, 2H), 6.63 (s, 2H), 3.97 (s, 6H), 3.91 (s, 4H), 3.45 (t, 2H, J = 7.3 Hz), 3.07 (br s, 2H), 2.65−2.57 (m, 4H), 1.90−1.88 (m, 4H), 1.63−1.58 (m, 4H), 1.36−1.35 (m, 4H). ^{13}C NMR ($CDCl_3$, 75 MHz): δ ppm 156.9, 155.7, 152.1, 151.1, 145.2, 145.2, 144.1, 130.1, 128.6, 128.0, 123.7, 123.3, 123.1, 122.9, 112.8, 112.8, 106.1, 105.5, 55.9, 53.1, 50.6, 49.3, 33.5, 29.7, 27.3, 26.8, 26.7, 24.6, 22.9, 22.6. IR (KBr): ν 3451, 2924, 2853, 1589, 1492, 1262, 750 cm^{-1}. MS (m/z): $[M + H]^+$ 618.2. HRMS (m/z): calcd for $C_{39}H_{44}N_3O_4$ $[M + H]^+$, 618.3326; found, 618.3302.

*N^1,N^1-Bis((7-methoxybenzofuran-2-yl)methyl)-N^6-(7,8,9,10-tetrahydro-6H-cyclohepta[b]quinolin-11-yl)hexane-1,6-diamine (**3d**).* Compound **3d** was prepared according to the general procedure II, yellow oil, yield 57%. ^1H NMR ($CDCl_3$, 300 MHz): δ ppm 7.96 (d, 2H, J = 8.4 Hz), 7.87 (dd, 1H, J = 8.4, 0.8 Hz), 7.59−7.53 (m, 1H), 7.42−7.36 (m, 1H), 7.15−7.08 (m, 4H), 6.78−6.69 (m, 2H), 6.63 (s, 2H), 3.98 (s, 6H), 3.91 (s, 4H), 3.25−3.15 (m, 4H), 2.89 (t, 2H, J = 5.3 Hz), 2.62−2.46 (m, 2H), 1.87−1.79 (m, 4H), 1.72−1.59 (m, 6H), 1.36−1.33 (m, 4H). ^{13}C NMR ($CDCl_3$, 75 MHz): δ ppm 156.9, 155.8, 152.1, 145.4, 145.0, 144.4, 130.3, 129.1, 128.4, 124.9, 124.0, 123.7, 123.4, 122.1, 113.2, 106.2, 105.6, 56.1, 53.4, 50.8, 50.7, 40.1, 32.1, 31.6, 29.8, 28.4, 27.8, 27.5, 27.1, 27.0. IR (KBr): ν 3445, 2926, 2853, 1586, 1462, 1266, 752 cm^{-1}. MS (m/z): 632.3 ($[M + H]^+$). HRMS (m/z): calcd for $C_{40}H_{44}N_3O_4$ $[M + H]^+$, 632.3483; found, 632.3474.

*N^1,N^1-Bis(benzofuran-2-ylmethyl)-N^7-(2,3-dihydro-1H-cyclopenta[b]quinolin-9-yl)heptane-1,7-diamine (**3e**).* Compound **3e** was prepared according to the general procedure II, yellow oil, yield 61%. ^1H NMR ($CDCl_3$, 300 MHz): δ ppm 8.02 (d, 1H, J = 8.3 Hz), 7.95 (d, 1H, J = 8.5 Hz), 7.57−7.52 (m, 3H), 7.47 (d, 2H, J = 7.7 Hz), 7.37 (t, 1H, J = 7.6 Hz), 7.26−7.17 (m, 4H), 6.62 (s, 2H), 6.32 (s, 1H), 3.88−3.83 (m, 4H), 3.65−3. 59 (m, 2H), 3.14 (q, 4H, J = 7.9 Hz), 2.59 (t, 2H, J = 7.2 Hz), 2.14 (q, 2H, J = 7.8 Hz), 1.67−1.60 (m, 4H), 1.34−1.26 (m, 6H). ^{13}C NMR ($CDCl_3$, 75 MHz): δ ppm 158.9, 157.3, 155.3, 151.2, 147.4, 129.3, 128.3, 126.1, 124.5, 123.8, 123.0, 122.6, 120.6, 118.1, 113.2, 111.2, 105.6, 53.4, 50.6, 45.4, 33.7, 31.2, 31.0, 29.7, 27.2, 27.1, 22.6, 23.0. IR(KBr): ν 3421, 2927, 2853, 1583, 1454, 1271, 752 cm^{-1}. MS (m/z): 558.3 ($[M + H]^+$). HRMS (m/z): calcd for $C_{37}H_{40}N_3O_2$ $[M + H]^+$, 558.3115; found, 558.3114.

*N^1,N^1-Bis(benzofuran-2-ylmethyl)-N^7-(1,2,3,4-tetrahydroacridin-9-yl)heptane-1,7-diamine (**3f**).* Compound **3f** was prepared according to the general procedure II, yellow oil, yield 42%. ^1H NMR ($CDCl_3$, 300 MHz): δ ppm 8.33 (d, 1H, J = 8.4 Hz), 8.08 (d, 1H, J = 8.6 Hz), 7.64 (t, 1H, J = 7.5 Hz), 7.53 (d, 2H, J = 7.0 Hz), 7.46 (d, 2H, J = 7.0 Hz), 7.39 (t, 1H, J = 7.8 Hz), 7.26−7.17 (m, 4H), 6.62 (s, 2H), 3.89 (s, 4H), 3.74 (t, 2H, J = 7.1 Hz), 3.22 (s, 2H), 2.63−2.57 (m, 4H), 1.89−1.81 (m, 4H), 1.72−1.69 (m, 4H), 1.34−1.26 (m, 6H). ^{13}C NMR ($CDCl_3$, 75 MHz): δ ppm 158.5, 157.1, 155.2, 151.2, 147.5, 131.1, 128.3, 124.7, 123.8, 123.7, 123.3, 122.6, 120.7, 117.0, 112.1, 111.2, 105.6, 53.3, 50.6, 48.9, 31.3, 30.1, 29.9, 27.2, 27.1, 26.6, 23.9, 22.2, 21.2. IR (KBr): ν 3421, 2929, 2855, 1583, 1453, 1254, 752 cm^{-1}. MS (m/z): 572.2 ($[M + H]^+$). HRMS (m/z): calcd for $C_{38}H_{42}N_3O_2$ $[M + H]^+$, 572.3272; found, 572.3257.

*N^1,N^1-Bis(benzofuran-2-ylmethyl)-N^7-(7,8,9,10-tetrahydro-6H-cyclohepta[b]quinolin-11-yl)heptane-1,7-diamine (**3g**).* Compound **3g** was prepared according to the general procedure II, pale-brown oil, yield 47%. ^1H NMR ($CDCl_3$, 300 MHz):): δ ppm 8.04 (d, 1H, J = 8.3 Hz), 7.89 (d, 1H, J = 8.4 Hz), 7.61−7.39 (m, 6H), 7.26−7.17 (m, 4H), 6.62 (s, 2H), 3.89 (s, 4H), 3.30 (t, 2H, J = 7.2 Hz), 3.23−3.20 (m, 2H), 2.91−2.88 (m, 2H), 2.59 (t, 2H, J = 7.3 Hz), 1.88−1.72 (m, 6H), 1.61−1.59 (m, 4H), 1.32−1.25 (m, 6H). ^{13}C NMR ($CDCl_3$, 75 MHz):

DOI: 10.1021/acs.jmedchem.5b01119
J. Med. Chem. 2016, 59, 114−131

δ ppm 156.9, 156.6, 152.2, 145.3, 145.0, 144.2, 128.3, 125.1, 123.8, 122.6, 122.0, 120.6, 111.2, 106.3, 105.5, 53.4, 50.6, 50.3, 38.8, 31.7, 31.4, 29.7, 29.1, 27.9, 27.5, 27.3, 27.1, 26.9, 26.6, 26.2. IR (KBr): ν 3420, 2925, 2854, 1589, 1271, 751 cm^{-1}. MS (*m*/*z*): 586.5 ($[M + H]^+$). HRMS (*m*/*z*): calcd for $C_{39}H_{44}N_3O_2$ $[M + H]^+$, 586.3428; found, 586.3415.

*N^1,N^1-Bis((7-methoxybenzofuran-2-yl)methyl)-N^7-(7,8,9,10-tetrahydro-6H-cyclohepta[b]quinolin-11-yl)heptane-1,7-diamine (**3h**).* Compound **3h** was prepared according to the general procedure II, pale-brown oil, yield 38%. ^1H NMR ($CDCl_3$, 300 MHz): δ ppm 8.21 (d, 1H, *J* = 8.1 Hz), 7.91 (d, 1H, *J* = 8.4 Hz), 7.62 (t, 1H, *J* = 7.7 Hz), 7.43 (t, 1H, *J* = 8.0 Hz), 7.12−7.11 (m, 4H), 6.77−6.74 (m, 2H), 6.63 (s, 2H), 3.99 (s, 6H), 3.91 (s, 4H), 3.39 (t, 2H, *J* = 7.0 Hz), 3.30−3.27 (m, 2H), 2.89−2.86 (m, 2H), 2.60 (t, 2H, *J* = 7.1 Hz), 1.88−1.81 (m, 4H), 1.71−1.54 (m, 6H), 1.32−1.25 (m, 6H). ^{13}C NMR ($CDCl_3$, 75 MHz): δ ppm 156.8, 156.6, 152.3, 145.1, 144.9, 144.1, 130.2, 129.8, 125.7, 125.3, 123.3, 122.6, 122.4, 122.2, 113.1, 106.2, 105.5, 56.0, 53.3, 50.6, 50.2, 36.5, 31.6, 31.3, 29.7, 29.0, 27.7, 27.3, 26.9, 26.8, 26.4. IR(KBr): ν 3421, 2923, 2851, 1582, 1493, 1266, 750 cm^{-1}. MS(*m*/*z*): 646.5 ($[M + H]^+$). HRMS (*m*/*z*): calcd for $C_{41}H_{48}N_3O_4$ $[M + H]^+$, 646.3649; found, 646.3616.

Determination of the 2e−*Tc*AChE Crystal Structure. *a. Crystallization.* *Tc*AChE was isolated, purified, and crystallized as previously described,[84] except for the affinity chromatography ligand, mono(aminocaproyl)-*p*-aminophenyltrimethylammonium. Because of its relatively limited solubility in water, **2e** was dissolved in DMSO (100 mM). The crystals of the complex were obtained by soaking the native crystals at 4 °C for 12 h in 2 mM **2e**, 30% PEG [poly(ethylene glycol)] 200, 8% DMSO, and 100 mM 2-(*N*-morpholino)-ethanesulfonic acid (MES) at pH 6.0.

b. Structure Determination. X-ray diffraction data were collected at the XRD-1 beamline of the Italian Synchrotron Facility ELETTRA (Trieste, Italy).[85] A PILATUS 2 M detector (Dectris Ltd., Baden, Switzerland) and focusing optics were employed for the measurements. The crystals were flash-cooled in a nitrogen stream at 100 K using an Oxford Cryosystems cooling device (Oxford, UK). Data were processed with MOSFLM version 7.0.7[86,87] and the CCP4 package version 6.3.0 software.[88] The enzyme−inhibitor structure was determined by Patterson search methods with the PHASER package version 2.3.0[89] using the refined coordinates of the native *Tc*AChE (PDB ID 1EA5)[53] after removal of the water molecules. Crystallographic refinement of the complex was performed with REFMAC version 5.7.[90] All data within the resolution range were included with no σ-cutoff. Bulk solvent correction and anisotropic scaling were applied. The Fourier maps were computed with σ-A weighted ($2|F_o| - |F_c|$, Φ_c) and ($|F_o| - |F_c|$, Φ_c) coefficients[91] after initial refinement of the native protein by the rigid body followed by maximum likelihood positional and individual isotropic temperature factor refinements. A prominent electron density feature in the catalytic gorge of *Tc*AChE and along the gorge itself allowed unambiguous fitting of the inhibitor. The initial Fourier difference map clearly indicated that a change occurred in the main-chain conformation of the loop encompassing residues Phe284 to Phe290 relative to its conformation in native *Tc*AChE. These residues were therefore removed from the model during the early rounds of refinement and refitted in stages as the refinement progressed, along with the respective side-chain orientations of residues within the Trp279 to Phe290 tract. Carbohydrates (*N*-acetyl β-D-glucosamine linked at Asn59, Asn416, and Asn457) were built in by inspecting electron density maps. Peaks in the difference Fourier maps that were greater than 1.8 rmsd were automatically added as water molecules to the atomic model and retained if they met stereochemical requirements, and their *B* factor were less than 80 $Å^2$ after refinement. Map inspection and model correction during refinement were based on the graphics program COOT version 0.7.[92] The crystal parameters, data collection, and refinement statistics are summarized in Supporting Information, Table S1. Figures were created using PyMOL version 1.7.2.1 (http://www.pymol.org).

Animal Studies. All experiments were performed in accordance with the National Institutes of Health Guide for the Care and Use of Laboratory Animals.[93] The procedures were approved by the Animal Care and Use Committee of the China Pharmaceutical University. The mice (ICR male mice, 8−10 weeks old, weight 20−25 g) were orally administered with tacrine and **2e** (20 μmol/kg body weight) 30 min before ip injection with scopolamine (1 mg/kg) or saline for 10 consecutive days. From the 11th day onward, the Morris water maze test was carried out 30 min after scopolamine injection.[94] Data for the escape latency, the distances traveled and the number of platform location crossings were collected by video equipment and processed by a computer equipped with an analysis-management system (Viewer2 Tracking Software, Ji Liang Instruments, Shanghai, China).

Behavioral Studies. The experiments were performed with adult male ICR mice (8−10 weeks old, weight 20−25 g), which were purchased from the Yangzhou University Medical Center (Yangzhou, China). Scopolamine hydrobromide was obtained from Aladdin Reagents (Shanghai, China). Tacrine was synthesized in the lab with >95% purity as determined by HPLC.

The mice were divided into four groups, and compounds were given to each group as follows: (i) vehicle, (ii) scopolamine, (iii) tacrine plus scopolamine, and (iv) compound **2e** plus scopolamine. Mice in groups (iii) and (iv) were orally administered with tacrine and **2e** (20 μmol/kg body weight), respectively, 30 min before the ip administration of scopolamine (1 mg/kg) or saline for 10 consecutive days.

Cognitive function was evaluated by the Morris water maze. The apparatus and test procedure have been previously described.[94] The test included 5 days of learning and memory training and a probe trial on day 6. Mice were individually trained in a circular pool (110 cm diameter, 60 cm height) filled to a depth of 40 cm with water at 25 °C. The maze was located in a lit room with visual cues. An escape platform (10 cm diameter) was placed in the center of one quadrant of the pool. The platform position was fixed, and the animal starting positions, facing the pool wall, were pseudorandomized for each trial. Each mouse was separately tested on both visible-platform (days 1−2) and hidden-platform (days 3−5) versions of the water maze. The hidden-platform version evaluates the spatial learning and was used to determine the retention of memory to find the platform. During the hidden-platform training trials, the escape platform was placed 1 cm below the surface of the water. On each day, the animal was subjected to three trials with a 20 min interval between trials. Each trial lasted for 90 s, unless the animal reached the platform before that time elapsed. The time taken for the mouse to reach the platform (a successful escape) was recorded. If an animal failed to find the platform within 90 s, the test ended and the animal was gently navigated to the platform by hand. Whether a mouse found or failed to find the platform within 90 s, it was kept on the platform for 30 s. On the last day (day 6), the platform was removed from its location and the animals were given a probe trial in which they had 90 s to search for the platform. The time taken to reach the missing platform and the number of times the animals crossed the platform location were recorded. All animals underwent nonspatial pretraining during the first two training days, which prepared them for the spatial learning test. During the visible trials of the water maze, mice were trained to find the platform, which was made visible to them by a small flag (5 cm tall).

Data for the escape latency, the distances traveled, and the number of platform location crossings were recorded and processed by an analysis-management system (Viewer2 Tracking Software, Ji Liang Instruments, China).

Hepatotoxicity Studies. The experiments were carried out on adult male ICR mice (weighing 18−22 g), which were purchased from the Yangzhou University Medicine Centre (Yangzhou, China). Tacrine was dissolved in a sodium carboxymethyl cellulose (CMC-Na) solution (0.5 g CMC-Na in 100 mL distilled water) and 30 mg/kg body wt, corresponding to 151.3 μmol/kg body wt., were given intragastrically (ig). Test compounds were dissolved in CMC-Na solution, and an equimolar dose corresponding to tacrine was administered ig. Heparinized serum was obtained 8, 22, and 36 h after dosing from the retrobulbar plexus to determine aspartate aminotransferase (ASAT) and alanine aminotransferase (ALT) activity, two indicators of liver damage, using routine colorimetric methods.[18,95]

DOI: 10.1021/acs.jmedchem.5b01119
J. Med. Chem. 2016, 59, 114−131

Statistics. The number of animals investigated per group for the biochemical investigations comprised n = 8−9. For behavioral studies, 9−10 mice per group were used. Results are expressed as the arithmetic means ± SD or means ± SEM. For statistical analyses, Student's *t* test was applied.

■ ASSOCIATED CONTENT

Supporting Information

The Supporting Information is available free of charge on the ACS Publications website at DOI: 10.1021/acs.jmedchem.5b01119.

Synthetic procedures and chemical characterization of the intermediates **4f** and **7**; *h*AChE and *h*BChE inhibition assay; kinetic analysis of *h*AChE inhibition; *Tc*AChE inhibition by compound **2e**; potentiometric titration of compound **2e** by *Tc*AChE; *h*AChE-induced $A\beta_{1-40}$ aggregation inhibition assay; inhibition of $A\beta_{1-42}$ self-aggregation. hBACE-1 inhibition assay; cell culture of the human neuroblastoma cell line SH-SY5Y; cell viability assay measured as reduction of MTT for derivatives **1h** and **3c**, crystallographic data collection and refinement statistics, kinetic studies for derivatives **1e**, **1f**, **1h**, and **3c** on *Tc*AChE; full and detailed results from animal studies; chromatographic determination of compounds purity; ^{1}H NMR, ^{13}C NMR, and HRMS spectra for N^1-(benzofuran-2-ylmethyl)-N^7-(1,2,3,4-tetrahydroacridin-9-yl)heptane-1,7-diamine (**2e**) (PDF)

Molecular formula strings (CSV)

Accession Codes

Atomic coordinates and structure factor amplitudes of the *Tc*AChE−**2e** complex have been deposited in the Brookhaven Protein Data Bank under the PDB ID code 4W63.

■ AUTHOR INFORMATION

Corresponding Authors

*For X.Z.: phone, +86-25-83271057; fax, +86-25-83271142; e-mail, xmzha@cpu.edu.cn.

*For M.B.: phone, +39-051-2099729; fax, 39-051-2099734; e-mail, manuela.bartolini3@unibo.it.

Author Contributions

¶X.Z. and D.L. contributed equally.

Notes

The authors declare no competing financial interest.

■ ACKNOWLEDGMENTS

X.Z. acknowledges the National Natural Science Foundation of China (nos. 30801428, 81273378), Specialized Research Fund for the Doctoral Program of Higher Education (no. 200803161011), the Natural Science Foundation of Jiangsu Province (no. BK2011622), and the Fundamental Research Funds for the Central Universities (no. ZJPZ2013001). M.B. and V.A. thank UniRimini S.p.A. and CIRI (POR FESR project). M.G.L. thanks the Spanish Ministry of Economy and Competence ref. SAF2013-32222 for the financial support. We also thank Dr. Andrea Milelli for useful discussion. X.Z. thanks Prof. Hao Hong (China Pharmaceutical University) and Dr. Susu Tang (China Pharmaceutical University) for their help in behavioral study. The authors also thank the staff of the XRD-1 beamline at Elettra-Sincrotrone Trieste S.C.p.A., Trieste, Italy, for assistance during data collection, Professor Israel Silman, Weizmann Institute of Science, Rehovot, Israel, for providing us with the purified *Tc*AChE used for the kinetics study, and Dr. Gregory E. Garcia, Research Division, U.S. Army Medical Research Institute of Chemical Defense (Aberdeen Proving Ground, MD, USA) for providing us with purified *Tc*AChE used for the structural study and for a fruitful long-term collaboration.

■ ABBREVIATIONS USED

AD, Alzheimer's disease; ACh, acetylcholine; ChEs, cholinesterases; AChE, acetylcholinesterase; BChE, butyrylcholinesterase; CAS, catalytic active site; PAS, peripheral anionic site; $A\beta$, β-amyloid; BACE-1, beta-secretase 1; ChEIs, cholinesterase inhibitors; MTDLs, multitarget-directed ligands; LAH, lithium aluminum hydride; THF, tetrahydrofuran; TLT, transfer latency time; ASAT, aspartate aminotransferase; ALT, alanine aminotransferase

■ REFERENCES

(1) Murphy, S. L.; Xu, J. Q.; Kochanek, K. D. *Deaths: Final Data for 2010*; National Center for Health Statistics: Hyattsville, MD, 2013.

(2) Rosini, M. Polypharmacology: the rise of multitarget drugs over combination therapies. *Future Med. Chem.* **2014**, *6*, 485−487.

(3) Leon, R.; Garcia, A. G.; Marco-Contelles, J. Recent advances in the multitarget-directed ligands approach for the treatment of Alzheimer's disease. *Med. Res. Rev.* **2013**, *33*, 139−189.

(4) Agis-Torres, A.; Sollhuber, M.; Fernandez, M.; Sanchez-Montero, J. M. Multi-target-directed ligands and other therapeutic strategies in the search of a real solution for Alzheimer's disease. *Curr. Neuropharmacol.* **2014**, *12*, 2−36.

(5) Bolea, I.; Gella, A.; Unzeta, M. Propargylamine-derived multitarget-directed ligands: fighting Alzheimer's disease with monoamine oxidase inhibitors. *J. Neural Transm.* **2013**, *120*, 893−902.

(6) Bartolini, M.; Bertucci, C.; Cavrini, V.; Andrisano, V. Beta-amyloid aggregation induced by human acetylcholinesterase: inhibition studies. *Biochem. Pharmacol.* **2003**, *65*, 407−416.

(7) Chacon, M. A.; Reyes, A. E.; Inestrosa, N. C. Acetylcholinesterase induces neuronal cell loss, astrocyte hypertrophy and behavioral deficits in mammalian hippocampus. *J. Neurochem.* **2003**, *87*, 195−204.

(8) Nitsch, R. M.; Slack, B. E.; Wurtman, R. J.; Growdon, J. H. Release of Alzheimer amyloid precursor derivatives stimulated by activation of muscarinic acetylcholine receptors. *Science* **1992**, *258*, 304−307.

(9) Peng, Y.; Jiang, L.; Lee, D. Y.; Schachter, S. C.; Ma, Z.; Lemere, C. A. Effects of huperzine A on amyloid precursor protein processing and beta-amyloid generation in human embryonic kidney 293 APP Swedish mutant cells. *J. Neurosci. Res.* **2006**, *84*, 903−911.

(10) Reale, M.; Di Nicola, M.; Velluto, L.; D'Angelo, C.; Costantini, E.; Lahiri, D. K.; Kamal, M. A.; Yu, Q. S.; Greig, N. H. Selective acetyl- and butyrylcholinesterase inhibitors reduce amyloid-beta ex vivo activation of peripheral chemo-cytokines from Alzheimer's disease subjects: exploring the cholinergic anti-inflammatory pathway. *Curr. Alzheimer Res.* **2014**, *11*, 608−622.

(11) Watkins, P. B.; Zimmerman, H. J.; Knapp, M. J.; Gracon, S. I.; Lewis, K. W. Hepatotoxic effects of tacrine administration in patients with Alzheimer's disease. *JAMA, J. Am. Med. Assoc.* **1994**, *271*, 992−998.

(12) Tumiatti, V.; Minarini, A.; Bolognesi, M. L.; Milelli, A.; Rosini, M.; Melchiorre, C. Tacrine derivatives and Alzheimer's disease. *Curr. Med. Chem.* **2010**, *17*, 1825−1838.

(13) Lupp, A.; Appenroth, D.; Fang, L.; Decker, M.; Lehmann, J.; Fleck, C. Tacrine-NO donor and tacrine-ferulic acid hybrid molecules as new anti-Alzheimer agents: hepatotoxicity and influence on the cytochrome P450 system in comparison to tacrine. *Arzneim. Forsch.* **2010**, *60*, 229−237.

(14) Romero, A.; Cacabelos, R.; Oset-Gasque, M. J.; Samadi, A.; Marco-Contelles, J. Novel tacrine-related drugs as potential candidates for the treatment of Alzheimer's disease. *Bioorg. Med. Chem. Lett.* **2013**, *23*, 1916−1922.

DOI: 10.1021/acs.jmedchem.5b01119
J. Med. Chem. 2016, 59, 114−131

(15) de Aquino, R. A. N.; Modolo, L. V.; Alves, R. B.; de Fatima, A. Design of new drugs for the treatment of Alzheimer's disease based on tacrine structure. *Curr. Drug Targets* **2013**, *14*, 378−397.
(16) Minarini, A.; Milelli, A.; Simoni, E.; Rosini, M.; Bolognesi, M. L.; Marchetti, C.; Tumiatti, V. Multifunctional tacrine derivatives in Alzheimer's disease. *Curr. Top. Med. Chem.* **2013**, *13*, 1771−1786.
(17) Nepovimova, E.; Uliassi, E.; Korabecny, J.; Pena-Altamira, L. E.; Samez, S.; Pesaresi, A.; Garcia, G. E.; Bartolini, M.; Andrisano, V.; Bergamini, C.; Fato, R.; Lamba, D.; Roberti, M.; Kuca, K.; Monti, B.; Bolognesi, M. L. Multitarget drug design strategy: quinone-tacrine hybrids designed to block amyloid-beta aggregation and to exert anticholinesterase and antioxidant effects. *J. Med. Chem.* **2014**, *57*, 8576−8589.
(18) Chen, Y.; Sun, J.; Fang, L.; Liu, M.; Peng, S.; Liao, H.; Lehmann, J.; Zhang, Y. Tacrine-ferulic acid-nitric oxide (NO) donor trihybrids as potent, multifunctional acetyl- and butyrylcholinesterase inhibitors. *J. Med. Chem.* **2012**, *55*, 4309−4321.
(19) Benchekroun, M.; Bartolini, M.; Egea, J.; Romero, A.; Soriano, E.; Pudlo, M.; Luzet, V.; Andrisano, V.; Jimeno, M. L.; Lopez, M. G.; Wehle, S.; Gharbi, T.; Refouvelet, B.; de Andres, L.; Herrera-Arozamena, C.; Monti, B.; Bolognesi, M. L.; Rodriguez-Franco, M. I.; Decker, M.; Marco-Contelles, J.; Ismaili, L. Novel tacrine-grafted Ugi adducts as multipotent anti-Alzheimer drugs: a synthetic renewal in tacrine-ferulic acid hybrids. *ChemMedChem* **2015**, *10*, 523−539.
(20) Esquivias-Perez, M.; Maalej, E.; Romero, A.; Chabchoub, F.; Samadi, A.; Marco-Contelles, J.; Oset-Gasque, M. J. Nontoxic and neuroprotective beta-naphthotacrines for Alzheimer's disease. *Chem. Res. Toxicol.* **2013**, *26*, 986−992.
(21) Ballard, C. G.; Greig, N. H.; Guillozet-Bongaarts, A. L.; Enz, A.; Darvesh, S. Cholinesterases: roles in the brain during health and disease. *Curr. Alzheimer Res.* **2005**, *2*, 307−318.
(22) Greig, N. H.; Utsuki, T.; Ingram, D. K.; Wang, Y.; Pepeu, G.; Scali, C.; Yu, Q. S.; Mamczarz, J.; Holloway, H. W.; Giordano, T.; Chen, D.; Furukawa, K.; Sambamurti, K.; Brossi, A.; Lahiri, D. K. Selective butyrylcholinesterase inhibition elevates brain acetylcholine, augments learning and lowers Alzheimer beta-amyloid peptide in rodent. *Proc. Natl. Acad. Sci. U. S. A.* **2005**, *102*, 17213−17218.
(23) Furukawa-Hibi, Y.; Alkam, T.; Nitta, A.; Matsuyama, A.; Mizoguchi, H.; Suzuki, K.; Moussaoui, S.; Yu, Q. S.; Greig, N. H.; Nagai, T.; Yamada, K. Butyrylcholinesterase inhibitors ameliorate cognitive dysfunction induced by amyloid-beta peptide in mice. *Behav. Brain Res.* **2011**, *225*, 222−229.
(24) Baharloo, F.; Moslemin, M. H.; Nadri, H.; Asadipour, A.; Mahdavi, M.; Emami, S.; Firoozpour, L.; Mohebat, R.; Shafiee, A.; Foroumadi, A. Benzofuran-derived benzylpyridinium bromides as potent acetylcholinesterase inhibitors. *Eur. J. Med. Chem.* **2015**, *93*, 196−201.
(25) Howlett, D. R.; Perry, A. E.; Godfrey, F.; Swatton, J. E.; Jennings, K. H.; Spitzfaden, C.; Wadsworth, H.; Wood, S. J.; Markwell, R. E. Inhibition of fibril formation in beta-amyloid peptide by a novel series of benzofurans. *Biochem. J.* **1999**, *340*, 283−289.
(26) Byun, J. H.; Kim, H.; Kim, Y.; Mook-Jung, I.; Kim, D. J.; Lee, W. K.; Yoo, K. H. Aminostyrylbenzofuran derivatives as potent inhibitors for Abeta fibril formation. *Bioorg. Med. Chem. Lett.* **2008**, *18*, 5591−5593.
(27) Ono, M.; Kung, M. P.; Hou, C.; Kung, H. F. Benzofuran derivatives as Abeta-aggregate-specific imaging agents for Alzheimer's disease. *Nucl. Med. Biol.* **2002**, *29*, 633−642.
(28) Allsop, D.; Gibson, G.; Martin, I. K.; Moore, S.; Turnbull, S.; Twyman, L. J. 3-p-Toluoyl-2-[4′-(3-diethylaminopropoxy)-phenyl]-benzofuran and 2-[4′-(3-diethylaminopropoxy)-phenyl]-benzofuran do not act as surfactants or micelles when inhibiting the aggregation of beta-amyloid peptide. *Bioorg. Med. Chem. Lett.* **2001**, *11*, 255−257.
(29) Rizzo, S.; Tarozzi, A.; Bartolini, M.; Da Costa, G.; Bisi, A.; Gobbi, S.; Belluti, F.; Ligresti, A.; Allara, M.; Monti, J. P.; Andrisano, V.; Di Marzo, V.; Hrelia, P.; Rampa, A. 2-Arylbenzofuran-based molecules as multipotent Alzheimer's disease modifying agents. *Eur. J. Med. Chem.* **2012**, *58*, 519−532.
(30) Sashidhara, K. V.; Modukuri, R. K.; Jadiya, P.; Dodda, R. P.; Kumar, M.; Sridhar, B.; Kumar, V.; Haque, R.; Siddiqi, M. I.; Nazir, A. Benzofuran-chalcone hybrids as potential multifunctional agents against Alzheimer's disease: synthesis and in vivo studies with transgenic caenorhabditis elegans. *ChemMedChem* **2014**, *9*, 2671−2684.
(31) Lee, S. H.; Kim, Y.; Kim, H. Y.; Kim, Y. H.; Kim, M. S.; Kong, J. Y.; Lee, M. H.; Kim, D. J.; Ahn, Y. G. Aminostyrylbenzofuran directly reduces oligomeric amyloid-beta and reverses cognitive deficits in Alzheimer transgenic mice. *PLoS One* **2014**, *9*, e95733.
(32) Yuan, J.; Venkatraman, S.; Zheng, Y.; McKeever, B. M.; Dillard, L. W.; Singh, S. B. Structure-based design of beta-site APP cleaving enzyme 1 (BACE1) inhibitors for the treatment of Alzheimer's disease. *J. Med. Chem.* **2013**, *56*, 4156−4180.
(33) Viayna, E.; Sola, I.; Bartolini, M.; De Simone, A.; Tapia-Rojas, C.; Serrano, F. G.; Sabate, R.; Juarez-Jimenez, J.; Perez, B.; Luque, F. J.; Andrisano, V.; Clos, M. V.; Inestrosa, N. C.; Munoz-Torrero, D. Synthesis and multitarget biological profiling of a novel family of rhein derivatives as disease-modifying anti-Alzheimer agents. *J. Med. Chem.* **2014**, *57*, 2549−2567.
(34) Ghosh, A. K.; Brindisi, M.; Tang, J. Developing beta-secretase inhibitors for treatment of Alzheimer's disease. *J. Neurochem.* **2012**, *120* (Suppl s1), 71−83.
(35) Li, S. Y.; Jiang, N.; Xie, S. S.; Wang, K. D.; Wang, X. B.; Kong, L. Y. Design, synthesis and evaluation of novel tacrine-rhein hybrids as multifunctional agents for the treatment of Alzheimer's disease. *Org. Biomol. Chem.* **2014**, *12*, 801−814.
(36) Szymanski, P.; Laznickova, A.; Laznicek, M.; Bajda, M.; Malawska, B.; Markowicz, M.; Mikiciuk-Olasik, E. 2,3-Dihydro-1H-cyclopenta[b]quinoline derivatives as acetylcholinesterase inhibitors-synthesis, radiolabeling and biodistribution. *Int. J. Mol. Sci.* **2012**, *13*, 10067−10090.
(37) Ronco, C.; Jean, L.; Outaabout, H.; Renard, P. Y. Palladium-catalyzed preparation of N-alkylated tacrine and huprine compounds. *Eur. J. Org. Chem.* **2011**, *2011*, 302−310.
(38) Baillie, S. E.; Bluemke, T. D.; Clegg, W.; Kennedy, A. R.; Klett, J.; Russo, L.; de Tullio, M.; Hevia, E. Potassium-alkyl magnesiates: synthesis, structures and Mg-H exchange applications of aromatic and heterocyclic substrates. *Chem. Commun.* **2014**, *50*, 12859−12862.
(39) Bondar, G.; Coish, P.; Lowe, D.; O'connor, S. J.; Shelekhin, T.; Smith, R. Preparation and use of biphenyl amino acid derivatives for the treatment of obesity. WO 2007016538 A2, 2007.
(40) Yu, W. Y.; Tsoi, Y. T.; Zhou, Z.; Chan, A. S. Palladium-catalyzed cross coupling reaction of benzyl bromides with diazoesters for stereoselective synthesis of (E)-alpha,beta-diarylacrylates. *Org. Lett.* **2009**, *11*, 469−472.
(41) Ellman, G. L.; Courtney, K. D.; Andres, V., Jr.; Feather-Stone, R. M. A new and rapid colorimetric determination of acetylcholinesterase activity. *Biochem. Pharmacol.* **1961**, *7*, 88−95.
(42) Pang, Y. P.; Quiram, P.; Jelacic, T.; Hong, F.; Brimijoin, S. Highly potent, selective, and low cost bis-tetrahydroaminacrine inhibitors of acetylcholinesterase. Steps toward novel drugs for treating Alzheimer's disease. *J. Biol. Chem.* **1996**, *271*, 23646−23649.
(43) Wang, H.; Carlier, P. R.; Ho, W. L.; Wu, D. C.; Lee, N. T.; Li, C. P.; Pang, Y. P.; Han, Y. F. Effects of bis(7)-tacrine, a novel anti-Alzheimer's agent, on rat brain AChE. *NeuroReport* **1999**, *10*, 789−793.
(44) Minarini, A.; Milelli, A.; Tumiatti, V.; Rosini, M.; Simoni, E.; Bolognesi, M. L.; Andrisano, V.; Bartolini, M.; Motori, E.; Angeloni, C.; Hrelia, S. Cystamine-tacrine dimer: a new multi-target-directed ligand as potential therapeutic agent for Alzheimer's disease treatment. *Neuropharmacology* **2012**, *62*, 997−1003.
(45) Fu, H.; Li, W.; Lao, Y.; Luo, J.; Lee, N. T.; Kan, K. K.; Tsang, H. W.; Tsim, K. W.; Pang, Y.; Li, Z.; Chang, D. C.; Li, M.; Han, Y. Bis(7)-tacrine attenuates beta amyloid-induced neuronal apoptosis by regulating L-type calcium channels. *J. Neurochem.* **2006**, *98*, 1400−1410.
(46) Xiao, X. Q.; Lee, N. T.; Carlier, P. R.; Pang, Y.; Han, Y. F. Bis(7)-tacrine, a promising anti-Alzheimer's agent, reduces hydrogen

DOI: 10.1021/acs.jmedchem.5b01119
J. Med. Chem. 2016, 59, 114−131

peroxide-induced injury in rat pheochromocytoma cells: comparison with tacrine. *Neurosci. Lett.* **2000**, *290*, 197−200.
(47) Hamulakova, S.; Janovec, L.; Hrabinova, M.; Spilovska, K.; Korabecny, J.; Kristian, P.; Kuca, K.; Imrich, J. Synthesis and biological evaluation of novel tacrine derivatives and tacrine-coumarin hybrids as cholinesterase inhibitors. *J. Med. Chem.* **2014**, *57*, 7073−7084.
(48) Hui, A.-L.; Chen, Y.; Zhu, S.-J.; Gan, C.-S.; Pan, J.; Zhou, A. Design and synthesis of tacrine-phenothiazine hybrids as multitarget drugs for Alzheimer's disease. *Med. Chem. Res.* **2014**, *23*, 3546−3557.
(49) Mesulam, M.; Guillozet, A.; Shaw, P.; Quinn, B. Widely spread butyrylcholinesterase can hydrolyze acetylcholine in the normal and Alzheimer brain. *Neurobiol. Dis.* **2002**, *9*, 88−93.
(50) Venneri, A.; McGeown, W. J.; Shanks, M. F. Empirical evidence of neuroprotection by dual cholinesterase inhibition in Alzheimer's disease. *NeuroReport* **2005**, *16*, 107−110.
(51) Greig, N. H.; Lahiri, D. K.; Sambamurti, K. Butyrylcholinesterase: an important new target in Alzheimer's disease therapy. *Int. Psychogeriatr.* **1999**, *14* (Suppl S1), 77−91.
(52) Inestrosa, N. C.; Dinamarca, M. C.; Alvarez, A. Amyloid-cholinesterase interactions. Implications for Alzheimer's disease. *FEBS J.* **2008**, *275*, 625−632.
(53) Dvir, H.; Jiang, H. L.; Wong, D. M.; Harel, M.; Chetrit, M.; He, X. C.; Jin, G. Y.; Yu, G. L.; Tang, X. C.; Silman, I.; Bai, D. L.; Sussman, J. L. X-ray structures of Torpedo californica acetylcholinesterase complexed with (+)-huperzine A and (−)-huperzine B: structural evidence for an active site rearrangement. *Biochemistry* **2002**, *41*, 10810−10818.
(54) Millard, C. B.; Kryger, G.; Ordentlich, A.; Greenblatt, H. M.; Harel, M.; Raves, M. L.; Segall, Y.; Barak, D.; Shafferman, A.; Silman, I.; Sussman, J. L. Crystal structures of aged phosphonylated acetylcholinesterase: nerve agent reaction products at the atomic level. *Biochemistry* **1999**, *38*, 7032−7039.
(55) Harel, M.; Schalk, I.; Ehret-Sabatier, L.; Bouet, F.; Goeldner, M.; Hirth, C.; Axelsen, P. H.; Silman, I.; Sussman, J. L. Quaternary ligand binding to aromatic residues in the active-site gorge of acetylcholinesterase. *Proc. Natl. Acad. Sci. U. S. A.* **1993**, *90*, 9031−9035.
(56) Rydberg, E. H.; Brumshtein, B.; Greenblatt, H. M.; Wong, D. M.; Shaya, D.; Williams, L. D.; Carlier, P. R.; Pang, Y. P.; Silman, I.; Sussman, J. L. Complexes of alkylene-linked tacrine dimers with Torpedo californica acetylcholinesterase: Binding of Bis5-tacrine produces a dramatic rearrangement in the active-site gorge. *J. Med. Chem.* **2006**, *49*, 5491−5500.
(57) Colletier, J. P.; Sanson, B.; Nachon, F.; Gabellieri, E.; Fattorusso, C.; Campiani, G.; Weik, M. Conformational flexibility in the peripheral site of *Torpedo californica* acetylcholinesterase revealed by the complex structure with a bifunctional inhibitor. *J. Am. Chem. Soc.* **2006**, *128*, 4526−4527.
(58) Desai, M. C.; Thadeio, P. F.; Lipinski, C. A.; Liston, D. R.; Spencer, R. W.; Williams, I. H. Physical parameters for brain uptake: optimizing log P, log D, and pKa of THA. *Bioorg. Med. Chem. Lett.* **1991**, *1*, 411−414.
(59) Greenblatt, H. M.; Guillou, C.; Guenard, D.; Argaman, A.; Botti, S.; Badet, B.; Thal, C.; Silman, I.; Sussman, J. L. The complex of a bivalent derivative of galanthamine with torpedo acetylcholinesterase displays drastic deformation of the active-site gorge: implications for structure-based drug design. *J. Am. Chem. Soc.* **2004**, *126*, 15405−15411.
(60) Morel, N.; Bon, S.; Greenblatt, H. M.; Van Belle, D.; Wodak, S. J.; Sussman, J. L.; Massoulie, J.; Silman, I. Effect of mutations within the peripheral anionic site on the stability of acetylcholinesterase. *Mol. Pharmacol.* **1999**, *55*, 982−992.
(61) Radic, Z.; Taylor, P. Interaction kinetics of reversible inhibitors and substrates with acetylcholinesterase and its fasciculin 2 complex. *J. Biol. Chem.* **2001**, *276*, 4622−4633.
(62) Bui, J. M.; Tai, K.; McCammon, J. A. Acetylcholinesterase: enhanced fluctuations and alternative routes to the active site in the complex with fasciculin-2. *J. Am. Chem. Soc.* **2004**, *126*, 7198−7205.
(63) Bui, J. M.; McCammon, J. A. Protein complex formation by acetylcholinesterase and the neurotoxin fasciculin-2 appears to involve an induced-fit mechanism. *Proc. Natl. Acad. Sci. U. S. A.* **2006**, *103*, 15451−15456.
(64) Castro, A.; Martinez, A. Targeting beta-amyloid pathogenesis through acetylcholinesterase inhibitors. *Curr. Pharm. Des.* **2006**, *12*, 4377−4387.
(65) Pi, R.; Mao, X.; Chao, X.; Cheng, Z.; Liu, M.; Duan, X.; Ye, M.; Chen, X.; Mei, Z.; Liu, P.; Li, W.; Han, Y. Tacrine-6-ferulic acid, a novel multifunctional dimer, inhibits amyloid-beta-mediated Alzheimer's disease-associated pathogenesis in vitro and in vivo. *PLoS One* **2012**, *7*, e31921.
(66) Yan, R.; Vassar, R. Targeting the beta secretase BACE1 for Alzheimer's disease therapy. *Lancet Neurol.* **2014**, *13*, 319−329.
(67) Ghosh, A. K.; Tang, J. Prospects of β-secretase inhibitors for the treatment of Alzheimer's Disease. *ChemMedChem* **2015**, *10*, 1463−1466.
(68) Hanessian, S.; Yun, H.; Hou, Y.; Yang, G.; Bayrakdarian, M.; Therrien, E.; Moitessier, N.; Roggo, S.; Veenstra, S.; Tintelnot-Blomley, M.; Rondeau, J. M.; Ostermeier, C.; Strauss, A.; Ramage, P.; Paganetti, P.; Neumann, U.; Betschart, C. Structure-based design, synthesis, and memapsin 2 (BACE) inhibitory activity of carbocyclic and heterocyclic peptidomimetics. *J. Med. Chem.* **2005**, *48*, 5175−5190.
(69) De Simone, A.; Mancini, F.; Real Fernandez, F.; Rovero, P.; Bertucci, C.; Andrisano, V. Surface plasmon resonance, fluorescence, and circular dichroism studies for the characterization of the binding of BACE-1 inhibitors. *Anal. Bioanal. Chem.* **2013**, *405*, 827−835.
(70) Willem, M.; Garratt, A. N.; Novak, B.; Citron, M.; Kaufmann, S.; Rittger, A.; DeStrooper, B.; Saftig, P.; Birchmeier, C.; Haass, C. Control of peripheral nerve myelination by the beta-secretase BACE1. *Science* **2006**, *314*, 664−666.
(71) Savonenko, A. V.; Melnikova, T.; Laird, F. M.; Stewart, K. A.; Price, D. L.; Wong, P. C. Alteration of BACE1-dependent NRG1/ErbB4 signaling and schizophrenia-like phenotypes in BACE1-null mice. *Proc. Natl. Acad. Sci. U. S. A.* **2008**, *105*, 5585−5590.
(72) Vassar, R. BACE1 inhibitor drugs in clinical trials for Alzheimer's disease. *Alzheimer's Res. Ther.* **2014**, *6*, 89.
(73) Ghosh, A. K.; Osswald, H. L. BACE1 (beta-secretase) inhibitors for the treatment of Alzheimer's disease. *Chem. Soc. Rev.* **2014**, *43*, 6765−6813.
(74) Cavalli, A.; Bolognesi, M. L.; Capsoni, S.; Andrisano, V.; Bartolini, M.; Margotti, E.; Cattaneo, A.; Recanatini, M.; Melchiorre, C. A small molecule targeting the multifactorial nature of Alzheimer's disease. *Angew. Chem., Int. Ed.* **2007**, *46*, 3689−3692.
(75) Prati, F.; De Simone, A.; Bisignano, P.; Armirotti, A.; Summa, M.; Pizzirani, D.; Scarpelli, R.; Perez, D. I.; Andrisano, V.; Perez-Castillo, A.; Monti, B.; Massenzio, F.; Polito, L.; Racchi, M.; Favia, A. D.; Bottegoni, G.; Martinez, A.; Bolognesi, M. L.; Cavalli, A. Multitarget drug discovery for Alzheimer's disease: triazinones as BACE-1 and GSK-3beta inhibitors. *Angew. Chem., Int. Ed.* **2015**, *54*, 1578−1582.
(76) Turner, R. T., 3rd; Hong, L.; Koelsch, G.; Ghosh, A. K.; Tang, J. Structural locations and functional roles of new subsites S5, S6, and S7 in memapsin 2 (beta-secretase). *Biochemistry* **2005**, *44*, 105−112.
(77) Fu, H.; Li, W.; Luo, J.; Lee, N. T.; Li, M.; Tsim, K. W.; Pang, Y.; Youdim, M. B.; Han, Y. Promising anti-Alzheimer's dimer bis(7)-tacrine reduces beta-amyloid generation by directly inhibiting BACE-1 activity. *Biochem. Biophys. Res. Commun.* **2008**, *366*, 631−636.
(78) Butterfield, D. A.; Swomley, A. M.; Sultana, R. Amyloid β-peptide (1−42)-induced oxidative stress in Alzheimer disease: importance in disease pathogenesis and progression. *Antioxid. Redox Signaling* **2013**, *19*, 823−835.
(79) Morris, R. Developments of a water-maze procedure for the studying spatial learning in the rat. *J. Neurosci. Methods* **1984**, *11*, 47−60.
(80) Ozer, J.; Ratner, M.; Shaw, M.; Bailey, W.; Schomaker, S. The current state of serum biomarkers of hepatotoxicity. *Toxicology* **2008**, *245*, 194−205.
(81) Dominguez, J. L.; Fernandez-Nieto, F.; Castro, M.; Catto, M.; Paleo, M. R.; Porto, S.; Sardina, F. J.; Brea, J.; Carotti, A.; Villaverde,

DOI: 10.1021/acs.jmedchem.5b01119
J. Med. Chem. 2016, 59, 114−131

M. C.; Sussman, F. S. Computer aided structure based design of multitarget leads for Alzheimer's disease. *J. Chem. Inf. Model.* **2014**, *55*, 135−148.
(82) Seubert, P.; Vigo-Pelfrey, C.; Esch, F.; Lee, M.; Dovey, H.; Davis, D.; Sinha, S.; Schiossmacher, M.; Whaley, J.; Swindlehurst, C.; et al. Isolation and quantification of soluble Alzheimer's beta-peptide from biological fluids. *Nature* **1992**, *359*, 325−327.
(83) Hu, M. K.; Wu, L. J.; Hsiao, G.; Yen, M. H. Homodimeric tacrine congeners as acetylcholinesterase inhibitors. *J. Med. Chem.* **2002**, *45*, 2277−2282.
(84) Sussman, J. L.; Harel, M.; Frolow, F.; Varon, L.; Toker, L.; Futerman, A. H.; Silman, I. Purification and crystallization of a dimeric form of acetylcholinesterase from Torpedo californica subsequent to solubilization with phosphatidylinositol-specific phospholipase C. *J. Mol. Biol.* **1988**, *203*, 821−823.
(85) Lausi, A.; Polentarutti, M.; Onesti, S.; Plaisier, J. R.; Busetto, E.; Bais, G.; Barba, L.; Cassetta, A.; Campi, G.; Lamba, D.; Pifferi, A.; Mande, S. C.; Sarma, D. D.; Sharma, S. M.; Paolucci, G. Status of the crystallography beamlines at Elettra. *Eur. Phys. J. Plus* **2015**, *130*, 43.
(86) Leslie, A. G. The integration of macromolecular diffraction data. *Acta Crystallogr., Sect. D: Biol. Crystallogr.* **2006**, *62*, 48−57.
(87) Battye, T. G.; Kontogiannis, L.; Johnson, O.; Powell, H. R.; Leslie, A. iMOSFLM: a new graphical interface for diffraction-image processing with MOSFLM. *Acta Crystallogr., Sect. D: Biol. Crystallogr.* **2011**, *67*, 271−281.
(88) Winn, M. D.; Ballard, C. C.; Cowtan, K. D.; Dodson, E. J.; Emsley, P.; Evans, P. R.; Keegan, R. M.; Krissinel, E. B.; Leslie, A. G.; McCoy, A.; McNicholas, S. J.; Murshudov, G. N.; Pannu, N. S.; Potterton, E. A.; Powell, H. R.; Read, R. J.; Vagin, A.; Wilson, K. S. Overview of the CCP4 suite and current developments. *Acta Crystallogr., Sect. D: Biol. Crystallogr.* **2011**, *67*, 235−242.
(89) McCoy, A. J.; Grosse-Kunstleve, R. W.; Adams, P. D.; Winn, M. D.; Storoni, L. C.; Read, R. J. Phaser crystallographic software. *J. Appl. Crystallogr.* **2007**, *40*, 658−674.
(90) Murshudov, G. N.; Skubák, P.; Lebedev, A. A.; Pannu, N. S.; Steiner, R. A.; Nicholls, R. A.; Winn, M. D.; Long, F.; Vagin, A. A. REFMAC5 for the refinement of macromolecular crystal structures. *Acta Crystallogr., Sect. D: Biol. Crystallogr.* **2011**, *67*, 355−367.
(91) Read, R. J. Improved Fourier coefficients for maps using phases from partial structures with errors. *Acta Crystallogr., Sect. A: Found. Crystallogr.* **1986**, *42*, 140−149.
(92) Emsley, P.; Lohkamp, B.; Scott, W. G.; Cowtan, K. Features and development of Coot. *Acta Crystallogr., Sect. D: Biol. Crystallogr.* **2010**, *66*, 486−501.
(93) National Research Council (US), Committee for the Update of the Guide for the Care and Use of Laboratory Animals *Guide for the Care and Use of Laboratory Animals*, 8th Ed.; The National Academies Press: Washington, DC, 2011.
(94) Xiang, G. Q.; Tang, S. S.; Jiang, L. Y.; Hong, H.; Li, Q.; Wang, C.; Wang, X. Y.; Zhang, T. T.; Yin, L. PPARgamma agonist pioglitazone improves scopolamine-induced memory impairment in mice. *J. Pharm. Pharmacol.* **2012**, *64*, 589−596.
(95) Doumas, B.; Biggs, H. G. A colorimetric method for assaying serum aspartate aminotransferase activities. *Clin. Chim. Acta* **1969**, *23*, 75−82.

DOI: 10.1021/acs.jmedchem.5b01119
J. Med. Chem. 2016, 59, 114−131